mCRE (Fig. 6A). The relative luciferase activities are 2.16-fold in mCRE/mNF-κB, 1.93-fold in mNF-κB/mNF-IL6, and 1.27-fold in mNF-IL6/mCRE. The cells transfected with triple-mutant (mNF-κB/mNF-IL6/mCRE) showed 0.80-fold luciferase activity (Fig. 6C). These results suggested that CRE, NF-κB, and NF-IL6 binding elements are all involved in the transcriptional activation of the COX-2 promoter mediated by heparanase, although the effect is not synergistic. Therefore, we used the other luciferase plasmids, pCRE-Luc and pNF-κB-Luc, which have multiple copies of CRE and NF-κB consensus binding elements, respectively (Mercury Pathway Profiling Luciferase System; Fig. 6B). Cells transfected with pNF-κB-Luc or pCRE-Luc showed 3.77- and 3.95-fold luciferase activity, respectively (Fig. 6C). These results suggest that heparanase increases the transcriptional activity of the COX-2 promoter and that this effect is likely to be dependent on all CRE, NF-κB, and NF-IL6 binding sites.

Discussion

Our results showed that heparanase and COX-2 are closely correlated with tumor malignancy through angiogenesis and that heparanase regulates the COX-2 expression. Immunohistochemical analysis revealed that heparanase and COX-2 proteins show very similar expression profile in esophageal cancer tissues, especially in tumor cells and stromal cells, such as fibroblasts, vascular endothelial cells, and inflammatory cells. Heparanase and COX-2 expression were located in the cytoplasm of tumor cells and highly correlated with depth of tumor invasion, lymph node metastasis, and lymphatic invasion. These findings support the notion that heparanase and COX-2 are involved in invasion and metastasis of malignant cells. Previous studies have shown that heparanase expression in esophageal cancer was significantly correlated with clinicopathologic variables and loss of syndecan-1 (34). In addition, the prognosis of patients with heparanase-positive and COX-2-positive tumors was significantly poorer than that of those with heparanase-negative and COX-2-negative tumors (3, 9, 12, 39). These results suggest that COX-2, as well as heparanase, is associated with tumor progression and prognosis in esophageal cancer.

Heparanase and COX-2 were also expressed strongly in stromal tissues adjacent to tumor tissues, such as vascular endothelial cells in angiogenic sprouts, fibroblasts, and inflammatory cells. Friedmann et al. (40) used immunohistochemical staining of human colon carcinoma tissue to show high expression of the heparanase protein in the endothelium of angiogenic sprouting capillaries but not of mature quiescent vessels. Masferrer et al. (41) showed that COX-2 immunoreactivity is associated with the microvasculature. These findings suggested that both heparanase and COX-2 are very important for cell-extracellular matrix interaction and that they may contribute to cancer progression. Therefore, we hypothesized that heparanase and COX-2 are linked to extracellular moieties and events, especially tumor angiogenesis. Tumor growth and

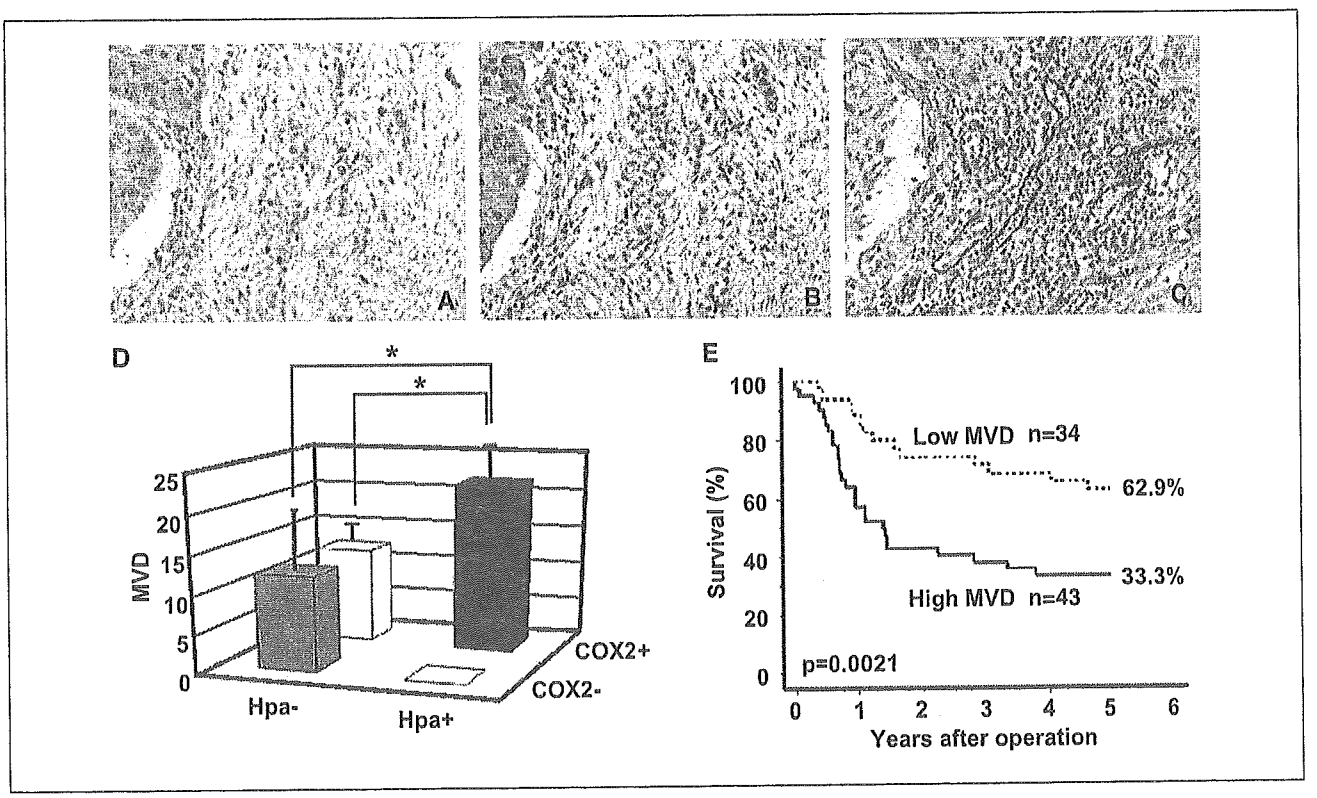

Fig. 3. Heparanase and COX-2 are expressed in vascular sprouts in intratumor tissue (*A* and *B*, respectively). Microvessels in tumor tissues detected by immunohistochemistry using anti-human von Willebrand factor (factor VIII) antibody (*C*). *D*, microvessel count in esophageal cancer according to expression of heparanase (*Hpa*) and COX-2. The MVD is shown against the heparanase and COX-2 expressions. *, $P < 0.005$. *E*, Kaplan-Meier survival curve of esophageal carcinoma patients with respect to MVD. High MVD patients show poor survival.

Table 2. Relationship with heparanase and COX-2 expression

A. Case no. in high and low MVD groups

	Low MVD (<18.6)*	High MVD (≥18.6)*	*P*
Heparanase (−)	20	4	0.0001
Heparanase (+)	14	39	
COX-2 (−)	17	4	0.0002
COX-2 (+)	17	39	

B. Mean value of MVD

	MVD†	*P*
Heparanase (−)	12.24 ± 7.85	<0.0001
Heparanase (+)	21.39 ± 6.45	
COX-2 (−)	12.21 ± 8.32	<0.0001
COX-2 (+)	20.90 ± 6.71	

C. Stage of esophageal squamous carcinomas

	Heparanase (−)	Heparanase (+)	*P*
T_{is}-T_{1b}			
COX-2 (−)	15	0	<0.0001
COX-2 (+)	2	12	
T_2-T_4			
COX-2 (−)	6	0	<0.0001
COX-2 (+)	1	41	
Total			
COX-2 (−)	21	0	<0.0001
COX-2 (+)	3	53	

NOTE: (−) and (+), absence and presence, respectively, of heparanase and COX-2 immunostainings.
*Mean MVD for all tumors was 18.6 ± 8.6.
†Mean ± SD.

metastasis depend on angiogenesis, which results from a cascade of molecular and cellular events that are involved n cell-extracellular matrix interactions (42). Degradation of extracellular matrix by matrix metalloproteinases and heparanase is a key process in cancer progression and facilitates neoangiogenesis. An important step in the angiogenic cascade is degradation of the subendothelial capillary basement membrane by proliferating endothelial cells, a prerequisite for the formation of vascular sprouts. HSPGs are prominent components of blood vessels. After degradation of HSPGs by heparanase, many angiogenic factors, such as basic FGF, transforming growth factor-β, heparin growth factor, and vascular endothelial growth factor, are released and activated. Elkin et al. (23) reported that recombinant heparanase released an active form of basic FGF and increased the angiogenic response. On the other hand, COX-2 is a rate-limiting enzyme involved in the conversion of arachidonic acid to prostaglandin H_2. The eicosanoids, especially prostaglandin E_2, are tightly associated with neovascularization and support vasculature-dependent solid tumor growth and metastasis. The tumorigenic effects of COX-2 could be divided into two distinct groups: the direct effect on tumor cells and the effect on nontumor cells, such as tumor-nurturing blood vessels and immunocompetent cells (43). Jones et al. (21) also showed that COX-2 inhibitors inhibited angiogenesis via direct effects in endothelial cell lines and that COX-2 was important for the direct regulation of angiogenesis in endothelial cells. Recent evidence has showed that COX-2 modulates angiogenesis either by augmenting the release of vascular endothelial growth factor, basic FGF, and nitric oxide by the tumor cells or by directly increasing production of prostaglandins (14, 44). In the present study, we analyzed MVD because it has been reported that heparanase and COX-2 are involved in angiogenesis as reflected by MVD (31, 39, 45). As shown in Fig. 3, in esophageal cancer patients, COX-2 and heparanase independently showed significant higher MVD. However, the immunopositivity of both heparanase and COX-2 showed the highest MVD, suggesting their additive function on angiogenesis. On the other hand, none of the heparanase-positive tumors were negative for COX-2, suggesting the inductive effect of heparanase on COX-2. Therefore, both heparanase and COX-2 might facilitate tumor angiogenesis, and these molecules might interact with each other. How does heparanase interact with COX-2? These two molecules showed similar expression pattern in both early and advanced stages of ESCCs significantly (Table 2C). The COX-2 mRNA and protein were up-regulated in heparanase-transfected esophageal cancer cells (Fig. 4). Therefore, we hypothesized that COX-2 acts downstream of heparanase and that the COX-2 promoter may contain heparanase-responsive regions.

COX-2 expression is differently regulated in various types of the cells (46) and also plays a key role in tumorigenesis (47). The COX-2 promoter contains three known consensus sequences for NF-κB, NF-IL6, and CRE, which are differently involved in the COX-2 promoter activity in different cells (37, 38, 48). In this study, we showed that combination of the CRE, NF-κB, and NF-IL6 site in the human *COX-2* gene was involved in promoter activity. Triple mutant (mNF-κB/mNF-IL6/mCRE) revealed remarkably reduced luciferase activity, whereas the destruction of the CRE, NF-κB, or NF-IL6 site alone showed no significant effect (Fig. 6C). The COX-2 promoter luciferase vectors containing double mutants of these sites also showed reduced promoter activity mediated by heparanase (Fig. 6C), although we could not exclude the possibility that the CRE, NF-κB, and NF-IL6 sites modulate the basal rather than the inducible promoter activity. It was reported that transcriptional regulation might be achieved through the cooperation of more than one *trans*-acting factor with the regulated assembly of multiprotein complexes on enhancers and promoters (49). The complex nature of these processes is thought to result in an elaborated fail-safe mechanism for controlling gene expression (49). Our results may be explained by the fail-safe mechanism of gene expression resulting from complex formation between transcription factors through the CRE, NF-κB, and NF-IL6 sites and other *cis*-acting element(s). Indeed, the promoter activity with mCRE and mNF-κB was increased as little as 2.57- and 2.44-fold, respectively, although those with multiple copies of CRE and NF-κB were increased ~3.95- and 3.77-fold, respectively (Fig. 6C). Based on these results, we inferred that NF-IL6 might be a component of a transcription factor

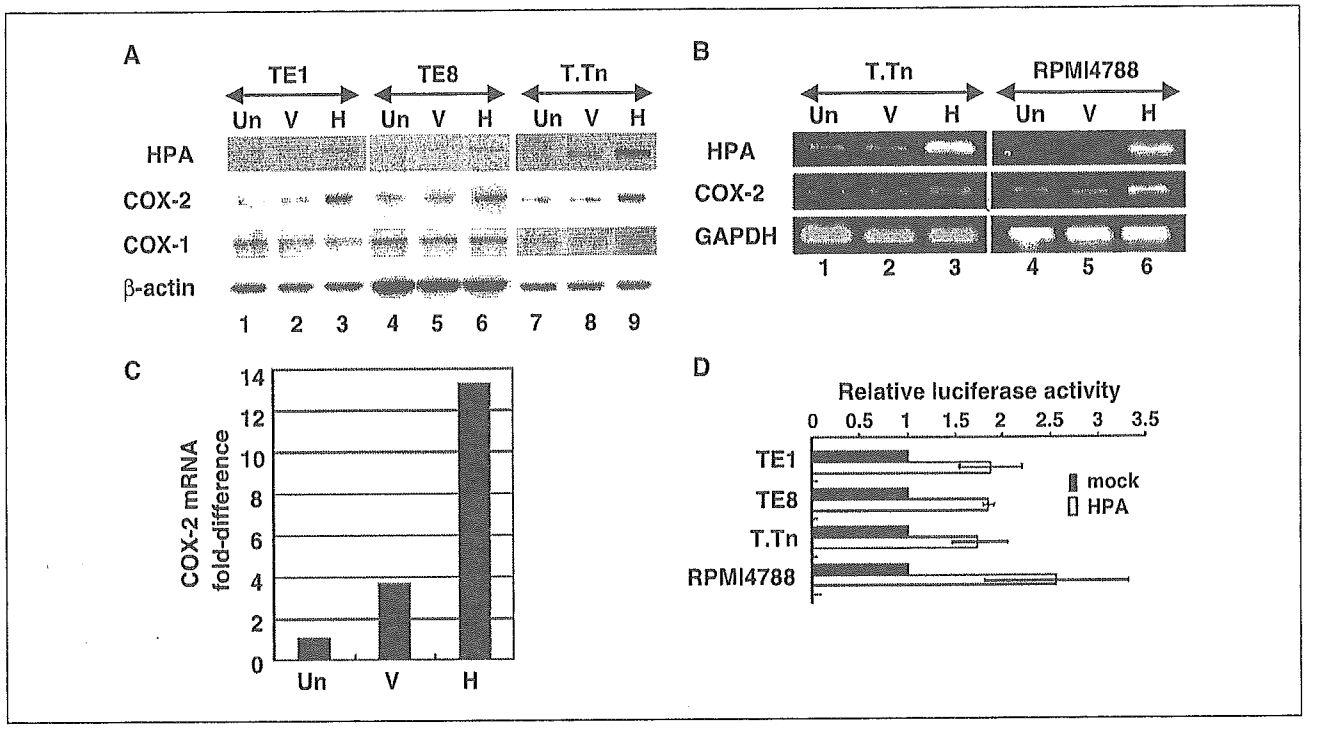

Fig. 4. Heparanase up-regulates COX-2 expression in cancer cell lines. *A*, Western blotting of esophageal squamous cancer cell lines, TE1 (*lanes 1-3*), TE8 (*lanes 4-6*), and T.Tn (*lanes 7-9*). COX-1 protein is shown as an internal control. *B*, heparanase cDNA-transfected T.Tn cells (*lane 3*) and RPMI4788 (*lane 6*) show increased COX-2 mRNA in comparison with parental and mock control (*lanes 1* and *2* for T.Tn and *lanes 4* and *5* for RPMI4788, respectively). *C*, up-regulation of the COX-2 mRNA in heparanase cDNA-transfected T.Tn cells by real-time PCR at 48 hours after transfection. The value in untransfected T.Tn cells is shown as 1. Un, untransfected cells; V, empty vector-only transfected cells; H, heparanase cDNA-transfected cells. *D*, relative luciferase activity is evaluated in TE1, TE8, T.Tn, and RPMI4788 cell lines using luciferase plasmid with COX-2 promoter (−1,432 to −59). Luciferase activity using empty vector (*mock*) is shown as 1. Each cell line shows higher luciferase activity in heparanase-transfected cells (*white columns*) than in mock control (*black columns*).

complex, which increased the COX-2 promoter activity mainly via the CRE and NF-κB, and that the increased promoter activity induced by the CRE and NF-κB might be finely regulated by other transcription factor(s) via the NF-IL6 site or other *cis*-acting element(s). The NF-IL6 site may be a candidate for such a *cis*-acting element, because NF-IL6 has been isolated as a *trans*-acting factor that binds to the p50 subunit of NF-κB (50). Our results using a series of truncated COX-2 promoters also suggest the existence of negative regulatory region on the −220 to −125 of the promoter. How the transcriptional regulation might work? Does heparanase bind directly to these sites or regulate other

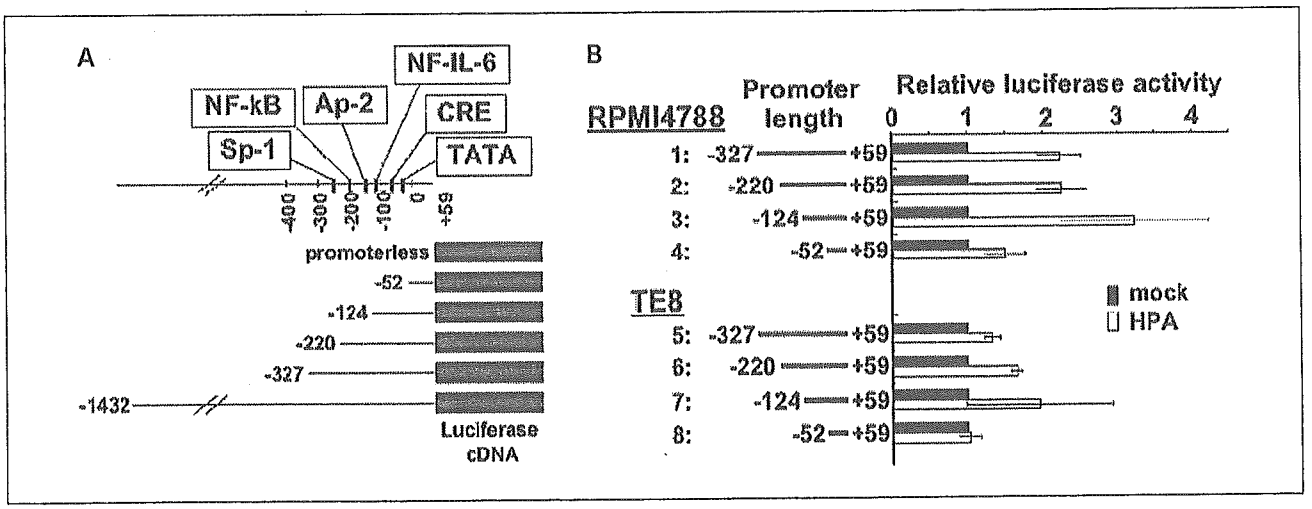

Fig. 5. *A*, schematic representation of reporter plasmids containing the human COX-2 promoter with truncation. *B*, transcriptional activity of the COX-2 promoters containing the regions of −327 to +59 (*lanes 1* and *5*), −224 to +59 (*lanes 2* and *6*), −120 to +59 (*lanes 3* and *7*), and −55 to +59 (*lanes 4* and *8*) in RPMI4788 cells (*lanes 1-4*) and TE8 cells (*lanes 5-8*).

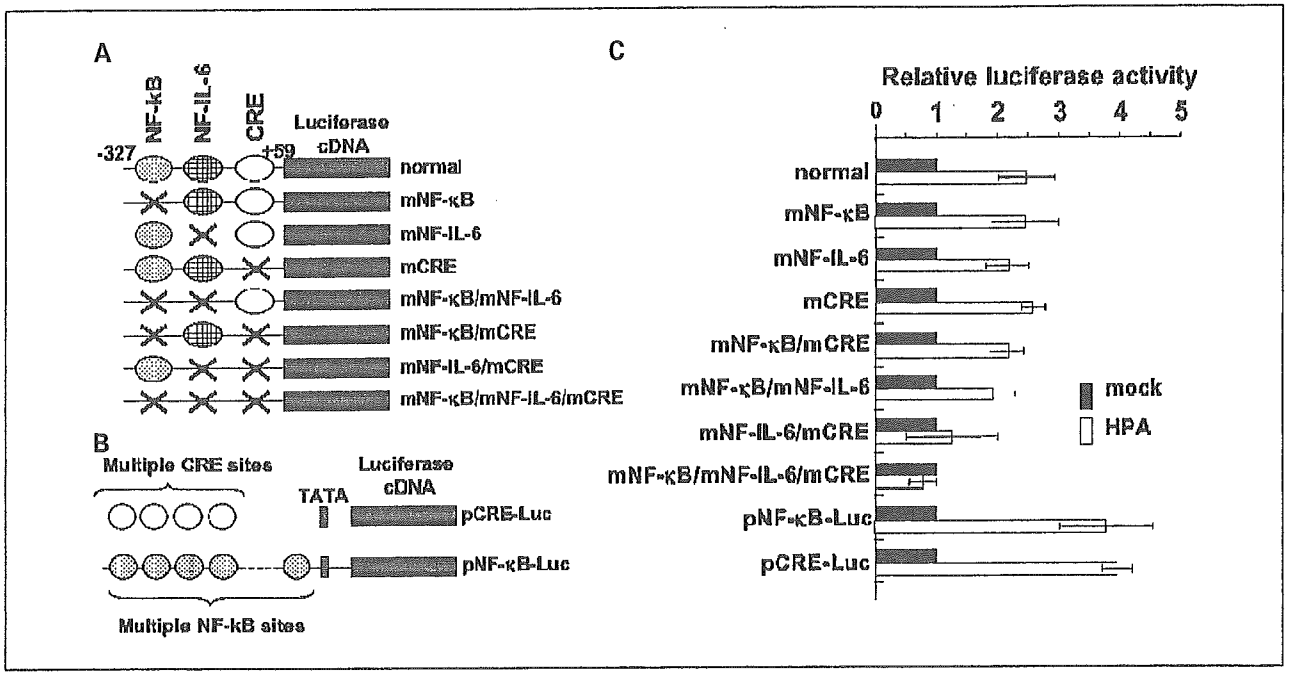

Fig. 6. *A* and *B*, schematic representation of reporter plasmids containing the mutant COX-2 promoters and consensus elements for NF-κB, mNF-IL6, and CRE (*A*) as well as pCRE-Luc and pNF-κB-Luc (*B*). The COX-2 promoter region (−327 to +59) was used for normal control (*lane 1*). *C*, relative luciferase activity. Columns, mean of four individual experiments; bars, SD.

molecules, which are linked to these transcription binding sites? We and others identified recently that the nuclear localization of heparanase and the presence of HSPGs in the nucleus are already known (35, 51). A recent study showed that nuclear heparanase degrades nuclear HSPGs, which may affect the transcriptional activity associated with FGF-2 (51). Although we currently do not have any direct or indirect proof about the relationship between heparan sulfate and the activities of transcriptional sites observed in our study, further analysis will clarify this point.

In conclusion, we showed that heparanase and COX-2 were tightly correlated with MVD and clinicopathologic features in esophageal cancers and that the COX-2 expression is up-regulated by heparanase. The expression pattern of the human *COX-2* gene is primarily accounted for by the transcriptional activity of the 5′ flanking region. The NF-κB and CRE sites were shown to be cooperatively involved in the *COX-2* gene promoter activity mediated by heparanase, although other *cis*-acting element(s), such as NF-IL6, may also be involved in this inducible promoter activity. Further analyses will be required to make clear the transcriptional mechanisms that are involved in activation of the COX-2 promoter by heparanase and their roles in tumorigenesis of esophageal cancers.

References

1. Eccles SA. Heparanase: breaking down barriers in tumors. Nat Med 1999;5:735–6.
2. Nakajima M, Irimura T, Di Ferrante N, Nicolson GL. Metastatic melanoma cell heparanase. Characterization of heparan sulfate degradation fragments produced by B16 melanoma endoglucuronidase. J Biol Chem 1984;259:2283–90.
3. Vlodavsky I, Friedmann Y, Elkin M, et al. Mammalian heparanase: gene cloning, expression and function in tumor progression and metastasis. Nat Med 1999;5:793–802.
4. Hulett MD, Freeman C, Hamdorf BJ, Baker RT, Harris MJ, Parish CR. Cloning of mammalian heparanase, an important enzyme in tumor invasion and metastasis. Nat Med 1999;5:803–9.
5. Parish CR, Freeman C, Hulett MD. Heparanase: a key enzyme involved in cell invasion. Biochim Biophys Acta 2001;1471:M99–108.
6. Nakajima M, Irimura T, Nicolson GL. Heparanases and tumor metastasis. J Cell Biochem 1988;36:157–67.
7. Nakajima M, Irimura T, Di Ferrante D, Di Ferrante N, Nicolson GL. Heparan sulfate degradation: relation to tumor invasive and metastatic properties of mouse B16 melanoma sublines. Science 1983;220:611–3.
8. Vlodavsky I, Ishai-Michaeli R, Mohsen M, Bar-Shavit R, Catane R, Ekre HP. Modulation of neovascularization and metastasis by species of heparin. Adv Exp Med Biol 1992;313:317–27.
9. Takaoka M, Naomoto Y, Ohkawa T, et al. Heparanase expression correlates with invasion and poor prognosis in gastric cancers. Lab Invest 2003;83:613–22.
10. Gohji K, Hirano H, Okamoto M, et al. Expression of three extracellular matrix degradative enzymes in bladder cancer. Int J Cancer 2001;95:295–301.
11. Ginath S, Menczer J, Friedmann Y, et al. Expression of heparanase, Mdm2, and erbB2 in ovarian cancer. Int J Oncol 2001;18:1133–44.
12. Rohloff J, Zinke J, Schoppmeyer K, et al. Heparanase expression is a prognostic indicator for postoperative survival in pancreatic adenocarcinoma. Br J Cancer 2002;86:1270–5.
13. Sheng H, Shao J, Morrow JD, Beauchamp RD, DuBois RN. Modulation of apoptosis and Bcl-2 expression by prostaglandin E_2 in human colon cancer cells. Cancer Res 1998;58:362–6.
14. Tsujii M, Kawano S, Tsuji S, Sawaoka H, Hori M, DuBois RN. Cyclooxygenase regulates angiogenesis induced by colon cancer cells. Cell 1998;93:705–16.
15. Tsujii M, Kawano S, DuBois RN. Cyclooxygenase-2 expression in human colon cancer cells increases metastatic potential. Proc Natl Acad Sci U S A 1997;94:3336–40.
16. Shattuck-Brandt RL, Lamps LW, Heppner Goss KJ, DuBois RN, Matrisian LM. Differential expression of matrilysin and cyclooxygenase-2 in intestinal and colorectal neoplasms. Mol Carcinog 1999;24:177–87.
17. Kambayashi T, Alexander HR, Fong M, Strassmann G. Potential involvement of IL-10 in suppressing tumor-associated macrophages. Colon-26-derived prostaglandin E_2 inhibits TNF-α release via a mechanism involving IL-10. J Immunol 1995;154:3383–90.
18. Shamma A, Yamamoto H, Doki Y, et al. Up-regulation of cyclooxygenase-2 in squamous carcinogenesis of the esophagus. Clin Cancer Res 2000;6:1229–38.

19. Wilson KT, Fu S, Ramanujam KS, Meltzer SJ. Increased expression of inducible nitric oxide synthase and cyclooxygenase-2 in Barrett's esophagus and associated adenocarcinomas. Cancer Res 1998;58:2929–34.
20. Leahy KM, Koki AT, Masferrer JL. Role of cyclooxygenases in angiogenesis. Curr Med Chem 2000;7:1163–70.
21. Jones MK, Wang H, Peskar BM, et al. Inhibition of angiogenesis by nonsteroidal anti-inflammatory drugs: insight into mechanisms and implications for cancer growth and ulcer healing. Nat Med 1999;5:1418–23.
22. Rapraeger AC, Krufka A, Olwin BB. Requirement of heparan sulfate for bFGF-mediated fibroblast growth and myoblast differentiation. Science 1991;252:1705–8.
23. Elkin M, Ilan N, Ishai-Michaeli R, et al. Heparanase as mediator of angiogenesis: mode of action. FASEB J 2001;15:1661–3.
24. Yayon A, Klagsbrun M, Esko JD, Leder P, Ornitz DM. Cell surface, heparin-like molecules are required for binding of basic fibroblast growth factor to its high affinity receptor. Cell 1991;64:841–8.
25. Vlodavsky I, Friedmann Y. Molecular properties and involvement of heparanase in cancer metastasis and angiogenesis. J Clin Invest 2001;108:341–7.
26. Boring CC, Squires TS, Tong T, Montgomery S. Cancer statistics, 1994. CA Cancer J Clin 1994;44:7–26.
27. Sagar PM, Gauperaa T, Sue-Ling H, McMahon MJ, Johnston D. An audit of the treatment of cancer of the oesophagus. Gut 1994;35:941–5.
28. Daly JM, Fry WA, Little AG, et al. Esophageal cancer: results of an American College of Surgeons Patient Care Evaluation Study. J Am Coll Surg 2000;190:562–72; discussion 572–3.
29. Kimura M, Haisa M, Uetsuka H, et al. TNF combined with IFN-α accelerates NF-κB-mediated apoptosis through enhancement of Fas expression in colon cancer cells. Cell Death Differ 2003;10:718–28.
30. Toyoshima M, Nakajima M. Human heparanase. Purification, characterization, cloning, and expression. J Biol Chem 1999;274:24153–60.
31. El-Assal ON, Yamanoi A, Ono T, Kohno H, Nagasue N. The clinicopathological significance of heparanase and basic fibroblast growth factor expressions in hepatocellular carcinoma. Clin Cancer Res 2001;7:1299–305.
32. Okada Y, Yamada S, Toyoshima M, Dong J, Nakajima M, Sugahara K. Structural recognition by recombinant human heparanase that plays critical roles in tumor metastasis: hierarchical sulfate groups with different effects and the essential target disulfated trisaccharide sequence. J Biol Chem 2002;277:42488–95.
33. Kutchera W, Jones DA, Matsunami N, et al. Prostaglandin H synthase 2 is expressed abnormally in human colon cancer: evidence for a transcriptional effect. Proc Natl Acad Sci U S A 1996;93:4816–20.
34. Mikami S, Ohashi K, Usui Y, et al. Loss of syndecan-1 and increased expression of heparanase in invasive esophageal carcinomas. Jpn J Cancer Res 2001;92:1062–73.
35. Ohkawa T, Naomoto Y, Takaoka M, et al. Localization of heparanase in esophageal cancer cells: respective roles in prognosis and differentiation. Lab Invest 2004;84:1289–304.
36. Inoue H, Nanayama T, Hara S, Yokoyama C, Tanabe T. The cyclic AMP response element plays an essential role in the expression of the human prostaglandin-endoperoxide synthase 2 gene in differentiated U937 monocytic cells. FEBS Lett 1994;350:51–4.
37. Inoue H, Yokoyama C, Hara S, Tone Y, Tanabe T. Transcriptional regulation of human prostaglandin-endoperoxide synthase-2 gene by lipopolysaccharide and phorbol ester in vascular endothelial cells. Involvement of both nuclear factor for interleukin-6 expression site and cAMP response element. J Biol Chem 1995;270:24965–71.
38. Shao J, Sheng H, Inoue H, Morrow JD, DuBois RN. Regulation of constitutive cyclooxygenase-2 expression in colon carcinoma cells. J Biol Chem 2000;275:33951–6.
39. Masunaga R, Kohno H, Dhar DK, et al. Cyclooxygenase-2 expression correlates with tumor neovascularization and prognosis in human colorectal carcinoma patients. Clin Cancer Res 2000;6:4064–8.
40. Friedmann Y, Vlodavsky I, Aingorn H, et al. Expression of heparanase in normal, dysplastic, and neoplastic human colonic mucosa and stroma. Evidence for its role in colonic tumorigenesis. Am J Pathol 2000;157:1167–75.
41. Masferrer JL, Leahy KM, Koki AT, et al. Antiangiogenic and antitumor activities of cyclooxygenase-2 inhibitors. Cancer Res 2000;60:1306–11.
42. Hanahan D, Folkman J. Patterns and emerging mechanisms of the angiogenic switch during tumorigenesis. Cell 1996;86:353–64.
43. Rahman MA, Dhar DK, Masunaga R, Yamanoi A, Kohno H, Nagasue N. Sulindac and exisulind exhibit a significant antiproliferative effect and induce apoptosis in human hepatocellular carcinoma cell lines. Cancer Res 2000;60:2085–9.
44. Form DM, Auerbach R. PGE_2 and angiogenesis. Proc Soc Exp Biol Med 1983;172:214–8.
45. Kelly T, Miao HQ, Yang Y, et al. High heparanase activity in multiple myeloma is associated with elevated microvessel density. Cancer Res 2003;63:8749–56.
46. Herschman HR. Prostaglandin synthase 2. Biochim Biophys Acta 1996;1299:125–40.
47. Oshima M, Dinchuk JE, Kargman SL, et al. Suppression of intestinal polyposis in ApcΔ716 knockout mice by inhibition of cyclooxygenase 2 (COX-2). Cell 1996;87:803–9.
48. Matsuura H, Sakaue M, Subbaramaiah K, et al. Regulation of cyclooxygenase-2 by interferon γ and transforming growth factor α in normal human epidermal keratinocytes and squamous carcinoma cells. Role of mitogen-activated protein kinases. J Biol Chem 1999;274:29138–48.
49. Tjian R, Maniatis T. Transcriptional activation: a complex puzzle with few easy pieces. Cell 1994;77:5–8.
50. LeClair KP, Blanar MA, Sharp PA. The p50 subunit of NF-κB associates with the NF-IL6 transcription factor. Proc Natl Acad Sci U S A 1992;89:8145–9.
51. Schubert SY, Ilan N, Shushy M, Ben-Izhak O, Vlodavsky I, Goldshmidt O. Human heparanase nuclear localization and enzymatic activity. Lab Invest 2004;84:535–44.

FEBS 30091 FEBS Letters 579 (2005) 6279–6287

ET-18-O-CH_3-induced apoptosis is causally linked to COX-2 upregulation in H-ras transformed human breast epithelial cells

Hye-Kyung Na[a], Hiroyasu Inoue[b], Young-Joon Surh[a,*]

[a] *National Research Laboratory of Molecular Carcinogenesis and Chemoprevention, College of Pharmacy, Seoul National University, Seoul 151-742, Republic of Korea*

[b] *South Korea and Department of Food Science and Nutrition, Nara Women's University, Nara, Japan*

Received 3 July 2005; accepted 10 September 2005

Available online 14 October 2005

Edited by Laszlo Nagy

Abstract **Abnormally elevated expression of cyclooxygenase-2 (COX-2) has been frequently observed in transformed or malignant cells, and certain non-steroidal anti-inflammatory drugs with COX-2 inhibitory activity exert anti-neoplastic or chemopreventive effects. Contrary to this notion, we have found that a novel alkylphospholipid type antitumor agent ET-18-O-CH_3 (1-*O*-octadecyl-2-*O*-methyl-glycero-3-phosphocholine) induces COX-2 expression in H-*ras* transformed human breast epithelial cells (MCF10A-*ras*) while it causes apoptosis at the same concentration range. The addition of a selective COX-2 inhibitor SC-58635 and *COX-2* gene knock down with the siRNA blocked ET-18-O-CH_3-induced apoptosis, suggesting that COX-2 induction by this drug is causally linked to its apoptosis inducing activity. ET-18-O-CH_3 enhanced the transcriptional activities of cyclic AMP response element which is a key regulator of COX-2 expression. 15-Deoxy-$\Delta^{12,14}$ prostaglandin J_2 is, an endogenous ligand for peroxisome proliferator-activated receptor γ (PPARγ), has been known to possess proapoptotic potential in diverse cell types. ET-18-O-CH_3 treatment resulted in elevated release of 15d-PGJ_2 and DNA binding and transcriptional activity of PPARγ. Based on these findings, it is likely that ET-18-O-CH_3 induces COX-2 expression and production of 15d-PGJ_2 which may mediate the ET-18-O-CH_3-induced apoptosis in MCF10A-*ras* cells.**

Keywords: Cyclooxygenase-2; Apoptosis; ET-18-O-CH_3; 15-Deoxy-$\Delta^{12,14}$-prostaglandin J_2; Human breast epithelial cells transformed with H-*ras* (MCF10A-*ras*)

1. Introduction

Cyclooxygenase (COX) initiates the conversion of arachidonate to a series of prostaglandins (PGs) and thromboxanes. Two isoforms of COX, i.e., COX-1 and COX-2, have been identified. COX-1, which is constitutively expressed in almost all tissues, is important for the maintenance of homeostatic functions, whereas COX-2, as an inducible isozyme, is transiently upregulated by pro-inflammatory cytokines, growth factors, tumor promoters, etc. [1]. Abnormal upregulation of COX-2 has been implicated in the pathogenesis of various human malignancies. There has been substantial body of data suggesting that COX-2 overexpression provides tumor cells with survival advantage leading to resistance to apoptosis and increased invasiveness or angiogenesis [2–4]. Conversely, selective COX-2 inhibitors have been shown to exert anti-carcinogenic activity [5,6]. Therefore, inhibition of COX-2 has been recognized as one of the most promising strategies for cancer prevention or treatment.

However, induction of COX-2 does not necessarily contribute to the cell survival or tolerance to proapoptotic insult. Thus, certain anticancer agents with pro-apoptotic activity were found to upregulate COX-2 expression in human hepatic myofibroblasts cells [7] and neuroglioma cells [8]. According to these studies, COX-2 inhibition by non-steroidal anti-inflammatory drugs (NSAID) blunted the anti-proliferative effect of these compound, suggesting that COX-2-derived PGs may be implicated in sensitizing these cells to apoptotic death. Moreover, in line with a possible proapoptotic function of COX-2, a major COX-2 product prostaglandin E_2 (PGE_2) [8] as well as 15-deoxy-$\Delta^{12,14}$-PGJ_2 (15d-PGJ_2) [9–11], a ligand of peroxisome proliferator-activated receptor γ (PPARγ), induced apoptosis in several types of cancer cells. Nonetheless, the molecular mechanism linking upregulation of COX-2 to induction of apoptosis has not been resolved yet.

ET-18-O-CH_3 (edelfosine; 1-*O*-octadecyl-2-*O*-methyl-*rac*-glycero-3-phosphocholine) is a synthetic analogue of 2-lysophosphatidylcholine that has been found to target cellular membranes and to exert potent anti-neoplastic effects [12,13]. ET-18-O-CH_3 has a broad spectrum of anti-tumorigenic effects [14–17]. The compound has been known to be a potent inducer of apoptosis in tumor cells, especially in leukemic cells, while sparing normal cells [18–20]. Inhibition of protein kinase C, phospholipase C, phosphatidylinositol 3-kinase, CTP: phosphocholine cytidylyltransferase, and coenzyme A-independent transacylase as well as blocking of arachidonate-phospholipid remodeling contributes to ET-18-O-CH_3-induced apoptosis [20–27]. ET-18-O-CH_3-induced apoptosis was accompanied by disruption of the mitochondrial transmembrane potential and activation of caspase-3 [15,28]. It also induces cell death by intracellular activation of the death receptor Fas/CD95 [18,29,30].

Here, we report that upregulation of COX-2 contributes to apoptotic death of the *ras*-transformed human mammary epithelial cells treated with the anti-cancer drug ET-18-O-CH_3.

2. Materials and methods

2.1. Materials

ET-18-O-CH_3 was purchased from BIOMOL Research Laboratories, Inc. (Plymouth Meeting, PA, USA). SC58635, a specific COX-2 inhibitor, was kindly provided by Pharmacia Korea. PGE_2 and

*Corresponding author. Fax: +82 2 874 9775.
E-mail address: surh@plaza.snu.ac.kr (Y.-J. Surh).

0014-5793/$30.00
doi:10.1016/j.febslet.2005.09.094

15d-PGJ_2 were obtained from Cayman Chemicals (Ann Arbor, MI, USA). Dulbecco's modified Eagle's medium (DMEM)/F-12, heat-inactivated horse serum, L-glutamine, and penicillin/streptomycin/fungizone mixture were products of Gibco-BRL (Grand Island, NY, USA). Insulin, cholera toxin, hydrocortisone, recombinant epidermal growth factor, and actin antibody were purchased from the Sigma Chemical Co. (St. Louis, MO, USA). Antibodies against poly(ADP-ribose)polymerase (PARP) and COX-2 were from Santa Cruz Biotechnology (Santa Cruz, CA, USA). Cleaved PARP antibody was purchased from Cell Signaling Technology (Beverly, MA, USA). Secondary antibodies were obtained from Zymed Laboratories Inc. (San Francisco, CA, USA). The ECL chemiluminescent detection reagent was purchased from Amersham Co. (Arlington Heights, IL, USA). A series of human COX-2 promoter deletion constructs ligated to luciferase gene were described previously [31]. The putative peroxisome-proliferator reactive element (PPRE) firefly luciferase reporter construct (pPPRE-Luc) was kindly provided by Dr. Kang-Yell Choi (Yonsei University, Seoul, Korea). [γ-^{32}P]ATP was the product of NEN Life Science (Boston, MA, USA). ET-18-O-CH_3 was dissolved in 50% ethanol. Other substances were dissolved in DMSO and was further diluted with culture medium.

2.2. Cell culture

The MCF10A cell line transfected with a virus carrying the H-*ras* oncogene (MCF10A-*ras*) was cultured as described previously [32]. The cells were cultured in DMEM/F-12 medium supplemented with 5% heat-inactivated horse serum, 10 μg/ml insulin, 100 ng/ml cholera toxin, 0.5 μg/ml hydrocortisone, 20 ng/ml recombinant EGF, 2 mM L-glutamine, and 100 μg/ml penicillin/streptomycin/fungi zone mixture at 37 °C in a 5% CO_2 atmosphere.

2.3. Cell growth assay

MCF10A-*ras* cells at 50–60% confluence were inoculated into the plate and exposed to the medium containing chemicals. The cell viability was determined by the trypan blue exclusion method or the conventional MTT reduction assay as described previously [16,33]. All samples were prepared in triplicates.

2.4. Measurement of PGs

MCF10A-*ras* cells cultured in 6-well plates were treated with ET-18-O-CH_3 with or without SC58635 for 3 days. The amounts of PGE_2 released into media were measured using the enzyme-immunoassay kit (Amersham Biosciences Corp., NJ, USA) according to the manufacturer's instructions. Briefly, 50 μl of culture medium previously centrifuged at 200 × *g* for 10 min was mixed with 50 μl PGE_2 antibody solution in the plate coated with goat anti-mouse IgG followed by incubation on ice for 3 h. After 50 μl horseradish peroxidase conjugate PGE_2 was added to the reaction mixture, the plate was kept on ice for additional 1 h. After aspiration and rinse four times with washing buffer, 150 μl of 3,3′,5,5′-tetramethylbenzidine substrate solution was added and incubation was continued for 30 min at room temperature in a dark place. The reaction was terminated by addition of 100 μl of 1 M sulfuric acid, and the absorbance at 450 nm was read by the ELISA reader. PGE_2 was quantitated using a standard curve constructed with known concentrations of PGE_2. Likewise, 15d-PGJ_2 was assayed using an enzyme immunoassay kit (Assay Designs Inc., Ann Arbor, MI, USA).

2.5. In situ nick end-labeling (TUNEL)

To detect apoptosis at a single cell level, enzymatic in situ nick end-labeling (TUNEL) was carried out with an in situ death detection kit (Boehringer Mannheim, Mannheim, Germany), according to a manufacture's protocol. Briefly, MCF10A-*ras* cells were cultured in a chamber slide™ in the absence or presence of ET-18-O-CH_3 for 3 days. The cells were fixed for 30 min in 10% neutral-buffered formalin solution at room temperature. Endogenous peroxidase was inactivated by incubation with 0.3% (v/v) hydrogen peroxide in methanol for 1 h at room temperature and further incubated in a permeabilizing solution (0.1% sodium citrate and 0.1% Triton X-100) for 2 min at 4 °C. The cells were labeled by incubation with the TUNEL reaction mixture for 60 min at 37 °C followed by labeling with peroxidase-conjugated anti-fluorescein anti-goat antibody (Fab fragment) for additional 30 min. After being stained with diaminobenzidine for 10 min, cells were rinsed with phosphate-buffered saline (PBS) and mounted with 50% glycerol.

2.6. Measurement of sub-diploid DNA

MCF10A-*ras* cells plated at a density of 2×10^5 cells in 6-well plates were treated with ET-18-O-CH_3 in the presence or absence of SC58635 for 24 h. The cells were washed, trypsinized, collected by centrifuged at 200 × *g* for 5 min, fixed with 1 ml of 70% cold ethanol and stored at −20 °C until use. After centrifugation at 1300 × *g* for 10 min, the fixed cells were stained with PBS containing 0.1% Triton X-100, 0.1 mM EDTA (pH 7.4), 10 μg/ml RNase A, and 50 μg/ml PI, and 10 000 cells per sample were analyzed by a FACScalibur instrument (Backton–Dicknson, USA). The DNA histograms were further analyzed by CellQuest Pro software to calculate the proportion of sub-diploid cell population.

2.7. Measurement of mitochondrial transmembrane potential

To measure the mitochondrial transmembrane potential ($\Delta\psi_m$), the lipophilic cationic probe TMRE was used. MCF10A-*ras* cells were cultured in 4 chamber slide glasses (Nunc, IL, USA). After treatment, the cells were rinsed with PBS and incubated with TMRE (150 nM) in the fresh media for 30 min at 37 °C. The cells were examined under a confocal microscope (Leica Microsystems Heidelberg GmbH, Heidelberg, Germany) with the fluorescence excitation at 488 nm and emission at 590 nm.

2.8. Western blot analysis

Treated MCF10A-*ras* cells were washed with PBS and harvested after digestion with lysis buffer (150 mM NaCl, 0.5% Triton X-100, 50 mM Tris–HCl, pH 7.4, 25 mM NaF, 20 mM EGTA, 1 mM DTT, 1 mM Na_3VO_4, protease inhibitor cocktail tablet). Cellular debris was removed by centrifugation at 23 000 × *g* for 15 min at 4 °C. The protein concentration was determined by using the BCA protein assay kit (Pierce Biotechnology, Inc., Rockford, IL). After addition of sample loading buffer, proteins were electrophoresed on a 12.5% SDS–polyacrylamide gel. The proteins were transferred to polyvinylidene difluoride membranes at 300 mA for 3 h. The membranes were blocked in 5% dried milk reconstituted in 0.1% Tween 20 in PBS (PBST). The blots were then incubated with primary antibodies (COX-2, PPARγ, caspase-3) in 3% dried milk/PBST. The blots were washed three times with PBST, and incubated with horseradish peroxidase-conjugated secondary antibodies in 3% dried milk/PBST for 1 h. The blots were washed again three times with PBST, and immunoreactive protein complexes were detected by the ECL detection reagent according to the manufacturer's instructions and visualized with X-ray film.

2.9. Reverse-transcriptase polymerase chain reaction (RT-PCR)

Total RNA was isolated from MCF10A-*ras* cells using TRIzol® (Invitrogen, Carlsbad, CA, USA). One μg of total RNA was reverse-transcribed with murine leukemia virus reverse transcriptase (Promega, Madison, WI, USA) at 42 °C for 50 min and 72 °C for 15 min. The cycling conditions were as follows: 3 min at 95 °C followed by 35 cycles of 95 °C, 30 s; 63 °C, 1 min; 72 °C, 1 min of COX-2; 26 cycles of 94 °C, 1 min; 63 °C, 2 min; 72 °C, 2 min of the house keeping gene, glyceraldehyde-3-phosphate dehydrogenase (GAPDH) followed by a final extension at 72 °C for 10 min. The primer pairs (forward and reverse, respectively) and the size of the expected products were as follows: COX-2, 5′-CGGGATCCATGCTCGCCCGCGCCCTGCTGC-3′ and 5′-GCTCTAGAGCCTACAGTTCAGTCGAACGTTC-3′, 1800 base pair; GAPDH, 5′-TGAAGGTCGGTGTCAACGGATTTGGC-3′ and 5′-CATGTAGGCCATGAGGTCCACCAC-3′, 983 base pair. Amplification products were analyzed on 1.2% agarose gel electrophoresis, stained with ethidium bromide, and photographed under ultraviolet light.

2.10. Transient transfection and the luciferase assay

MCF10A-*ras* cells seeded at a density of 2×10^5/well in a 6-well dish were grown to 60–70% confluence in complete growth media. The cells were co-transfected with 2 μg of plasmid DNA constructs and 0.5 μg of pCMV-β galactosidase control vector with DOTAP liposomal transfection reagent (Roche Applied Science, Mannheim, Germany) according to the manufacturer's instructions. After 12-h transfection, the cells were treated with ET-18-O-CH_3 for additional 6 h and then washed

with PBS and lysed in 1× reporter lysis buffer (Promega, Madison, WI). The activities of firefly luciferase in the cell lysates were measured using the luciferase reporter assay system according to the manufacturer's instructions (Promega, Madison, WI) by Luminoskan luminometer (Thermo Labsystems, Helsinki, Finland). β-Galactosidase activity was measured by using the commercially available assay kit (Promega, Madison, WI). The relative luciferase activity was obtained by normalizing the firefly luciferase activity against the β-galactosidase activity.

2.11. COX-2 siRNA transfection

An oligonucleotide sequence for COX-2 siRNA was selected to knock down COX-2 expression by utilizing the siRNA Target Finder software at www.invitrogen.com. The human COX-2 specific siRNA (5′-AAG GGC UCU AGU AUA AUA GGA GAG G-3′) and the non-specific siRNA (5′-AAG AGG GCU CGA UUA UUA AGG AGG G-3′) were provided by Invitrogen (Carlsbad, CA, USA). MCF10A-*ras* cells were transfected with an oligonucleotide sequence for COX-2 siRNA or non-specific siRNA for 24 h with DOTAP liposomal transfection reagent (Roche Applied Science, Mannheim, Germany) according to the manufacturer's instructions. After 24 h transfection, the cells were treated with ET-18-O-CH_3 or vehicle alone for 6 h.

2.12. Preparation of nuclear extracts

MCF10A-*ras* cells were cultured in 100-mm dishes in the absence or presence of ET-18-O-CH_3. Cells were gently washed with cold PBS, scraped, and centrifuged at 1300 × *g* for 5 min. Pellets were suspended in cold hypotonic buffer [10 mM HEPES, pH 7.9, 1.5 mM $MgCl_2$, 0.3 mM EDTA, 0.1 mM phenylmethylsulfonylfluoride (PMSF)]. The lysates were incubated for 10 min on ice and then centrifuged at 20200 × *g* for 15 min at 4 °C. The pellets were washed with hypotonic buffer and resuspended in hypertonic buffer (30 mM HEPES, 1.5 mM $MgCl_2$, 0.3 mM EDTA, 10% glycerol, 450 mM NaCl, 0.1 mM PMSF) in ice for 30 min during rocking followed by centrifugation at 20200 × *g* for 15 min. After determination of the protein concentration, the supernatant was stored at −80 °C before use.

2.13. Electrophoretic mobility shifty assay

The oligonucleotides harboring the PPRE consensus sequence (5′-CCAAGGTCAAAGGT-3′) were end-labeled with [γ-^{32}P] ATP using T4 polynucleotide kinase (Takara, Japan). The nuclear protein (7–10 μg) was incubated with 8.5 μl of incubation buffer (30 mM HEPES, pH 7.9, 1.5 mM $MgCl_2$, 0.3 mM EDTA, pH 8.0, 10% glycerol), 2.5 μl polydI-dC (0.5 μg/μl), and the hypertonic buffer was added up to 20 μl of total volume. The reaction mixture was preincubated at room temperature for 15 min. The labeled oligonucleotide (50000–100000 cpm) was added and incubated for 30 min at room temperature for DNA-binding reactions. To ensure the specificity of the binding, a competition experiment was carried out by adding the excess unlabeled oligonucleotide to the reaction mixture before addition of the labeled oligonucleotide. Samples were separated on the 6% acrylamide gels at 150 mA in 0.25× tris–borate–EDTA buffer. After vacuum-dried, the gel was exposed to X-ray film for autoradiography at −70 °C.

3. Results

3.1. ET-18-O-CH_3-induced apoptosis in MCF10A-ras cells

Treatment of MCF10A-*ras* cells with ET-18-O-CH_3 inhibited the cell growth in a concentration dependent manner (Fig. 1A). ET-18-O-CH_3 treatment resulted in distinct morphological changes including rapid blebbing of plasma membrane and nuclear disintegration that are characteristic of apoptotic cell death (Fig. 1B). Moreover, MCF10A-*ras* cells treated with ET-18-O-CH_3 exhibited proteolytic cleavage of caspase-3 and the DNA repair enzyme PARP that are typical biochemical changes frequently observed in cells undergoing apoptotic death (Fig. 1C).

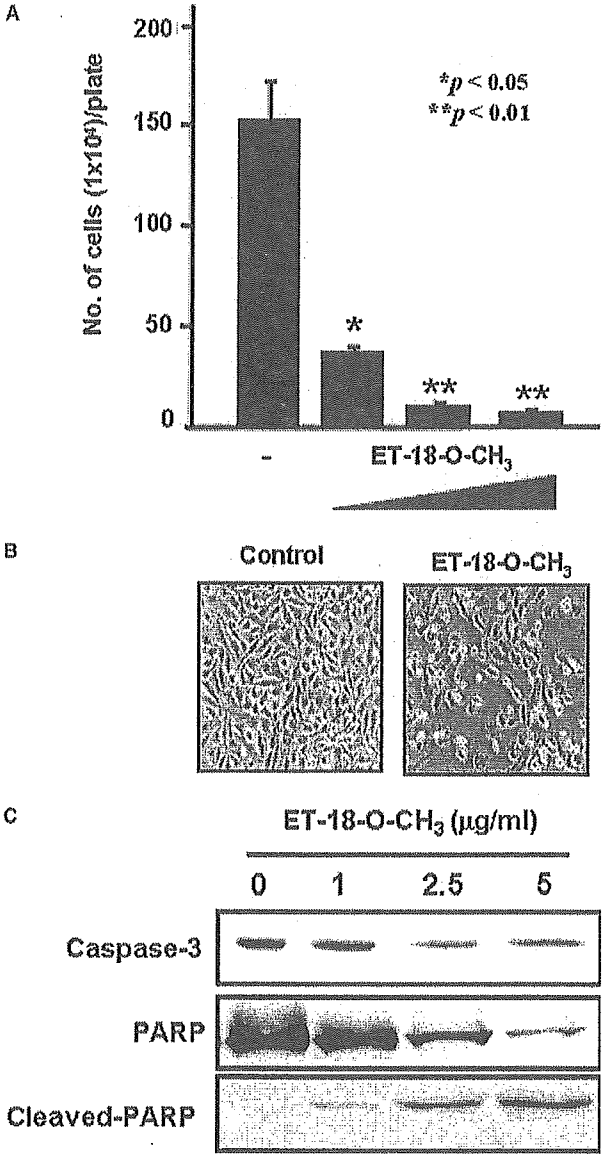

Fig. 1. Effects of ET-18-O-CH_3 on growth of MCF10A-*ras* cells. (A) The trypan blue dye exclusion method. Ten thousands of MCF10A-*ras* cells were inoculated into 35-mm dishes and exposed to the medium for 3 days with various concentrations (0, 1, 2.5, 5 μg/ml) of ET-18-O-CH_3. Treated cells were trypsinized followed by staining with trypan blue, and viable cells were counted by a hematocytometer. Bars represent means ± S.E.M. of triplicate experiments. A significant difference in the relative viability between treated cells and solvent controls is indicated with an asterisk. (B) Morphological changes in the MCF10A-*ras* cells treated with ET-18-O-CH_3 (2.5 μg/ml) for 1 day. Visualized by phase-contrast microscopy. (C) ET-18-O-CH_3-induced proteolytic cleavage of caspase-3 and PARP. MCF10A-*ras* cells were exposed to indicated concentrations of ET-18-O-CH_3 for 3 days. Protein from cell lysates was resolved by SDS–PAGE by Western blot using antibodies against caspase-3, PARP, and cleaved-PARP.

3.2. ET-18-O-CH_3 upregulated COX-2 expression while inducing apoptosis

Activated *ras* oncogene has been associated with upregulation of COX-2 in breast cancer cells [34], colorectal adenomas [35,36] and non-small cell lung cancer [37]. In recognition of this notion, we attempted to determine whether ET-18-O-CH_3 could induce apoptosis through downregulation of

COX-2 expression. Contrary to our expectation, ET-18-O-CH_3-induced COX-2 expression at both protein and mRNA levels in a concentration dependent manner, whereas basal COX-2 expression in MCF10A-*ras* cells remained relatively low (Fig. 2A and B). Unlike COX-2, the expression of COX-1 was not affected by ET-18-O-CH_3 treatment in MCF10A-*ras* cells (data not shown). In parallel with elevated COX-2 expression, PGE_2 production was also significantly increased upon ET-18-O-CH_3 treatment (Fig. 2C).

3.3. Upregulation of COX-2 was causally linked to ET-18-O-CH_3-induced apoptosis in MCF10A-ras cells

Although upregulation of COX-2 expression has been frequently associated with resistance to apoptosis, ET-18-O-CH_3-induced apoptosis and COX-2 expression in MCF10A-*ras* cells under the same experiment conditions. To examine whether ET-18-O-CH_3-induced COX-2 expression contributes to induction of apoptosis, a selective COX-2 inhibitor SC58635 was utilized. SC58635 inhibited ET-18-O-CH_3-induced production of PGE_2 in MCF10A-*ras* cells (Fig. 3A). We observed that SC58635, at a concentration that blocks COX-2, protected MCF10A-*ras* from ET-18-O-CH_3-induced proteolytic cleavage of caspase-3 (Fig. 3B). The same concentration of SC58635 inhibited the ET-18-O-CH_3-induced DNA fragmentation and lowered the sub G_0/G_1 proportion as measured by TUNEL staining and flow cytometry, respectively (Fig. 3C). The pharmacologic inhibition of COX-2 also restored the mitochondrial transmembrane potential ($\Delta\psi_m$) which was perturbed in ET-18-O-CH_3 treated cells (Fig. 3C). Likewise, the ET-18-O-CH_3-induced PARP cleavage was abolished upon direct *COX-2* gene knock down by employing the COX-2 siRNA (Fig. 3D), lending further support to the notion that upregulation of COX-2 expression is causally linked to induction of apoptosis in MCF10A-*ras* cells.

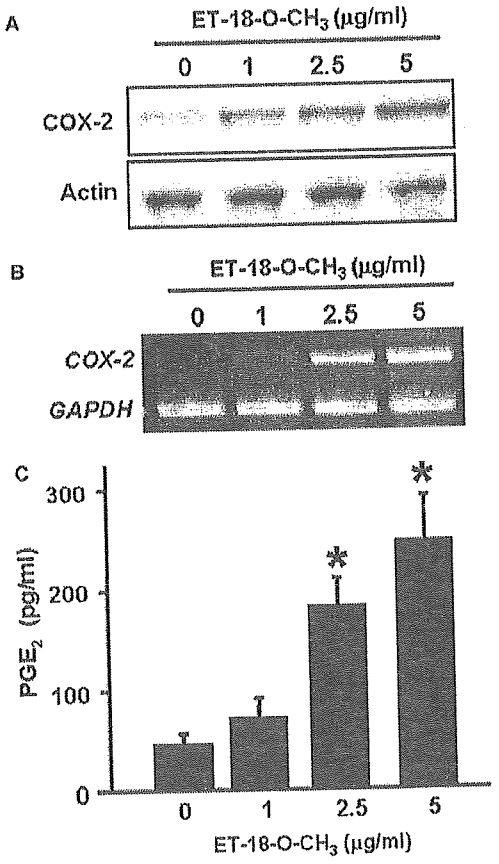

Fig. 2. Effects of ET-18-O-CH_3 on expression of COX-2 and PGE_2 production in MCF10A-*ras* cells. (A) Western blot analysis of COX-2 protein expression. MCF10A-*ras* cells were treated with various concentrations of ET-18-O-CH_3 for 3 days. Protein extracts from the cells were immunoblotted with anti-COX-2 antibody. (B) Determination of the relative amount of *COX-2* mRNA. Total RNA was extracted with TRIzol®, and RT-PCR for COX-2 mRNA transcripts was carried out as described under Section 2.9. GAPDH was used as an equal loading control. (C) ET-18-O-CH_3-induced PGE_2 production in MCF10A-*ras* cells. PGE_2 production was measured 3 days later by using the PGE_2 enzyme immunoassay kit following the manufacturer's protocol. A significant difference between treated cells and solvent controls is indicated with an asterisk ($P < 0.01$).

3.4. ET-18-O-CH_3 enhanced the COX-2 promoter activity

The regulation of COX-2 synthesis occurs mainly at the transcriptional level, although mRNA stabilization is also involved in response to specific signals. The types and nature of stimuli, signal transduction pathways, and transcription factors involved in the induction of *COX-2* gene expression are extremely diversified and cell specific. Several *cis*-acting elements are found in the COX-2 promoter, such as nuclear factor-κB (NF-κB), nuclear factor-interleukin-6 (NF-IL6), cyclic AMP response element (CRE), and E-box [38,39]. In order to determine which transcription factors are involved in ET-18-O-CH_3-induced COX-2 expression, MCF10A-*ras* cells were transiently transfected with human COX-2 promoter luciferase constructs (−1432/+59) (Fig. 4A) and challenged with ET-18-O-CH_3 for 6 h. Treatment with ET-18-O-CH_3 resulted in about a 6-fold increase in the *COX-2* promoter (−1432/+59) activity. To elucidate the critical region of the COX-2 promoter responsible for COX-2 expression by ET-18-O-CH_3, we utilized a series of *COX-2* deletion constructs (−1432/+59, −327/+59, −220/+59, −124/+59, and −52/+59). The *COX-2* promoter activity was most prominent when the −327/+59 promoter construct was used (Fig. 4B). As the promoter length was shortened, COX-2 activities were diminished gradually. It is noticeable that the −52/+59 construct exhibited an approximately 97% loss of the *COX-2* promoter activity compared with the −327/+59 construct. A CRE is present between nucleotides −59 and −53, suggesting that this element might responsible for mediating the COX-2 inducing effects of ET-18-O-CH_3. To precisely define which of these *cis*-acting elements are involved in ET-18-O-CH_3-induced *COX-2* promoter activity, MCF10A-*ras* cells were transiently transfected with site-specific mutant *COX-2* promoter constructs. As shown in Fig. 4C, CRM (−327/+59 construct in which mutated at the CRE site) significantly decreased the *COX-2* promoter activity in ET-18-O-CH_3-treated cells. The introduction of ILM (mutated at the NF-IL6 site) resulted in approximately 2-fold reduction, compared with the wild type −327/+59 construct while little effect on *COX-2* promoter activity was achieved with KBM (mutated at the NF-κB site) (Fig. 4C). These results suggest that CRE and possibly NF-IL6 play important role in mediating the induction of COX-2 gene expression.

3.5. ET-18-O-CH_3 induced production of 15d-PGJ_2 and expression as well as activation of PPARγ

To clarify how COX-2 upregulation by ET-18-O-CH_3 leads to induction of apoptosis in MCF10A-*ras* cells, we attempted

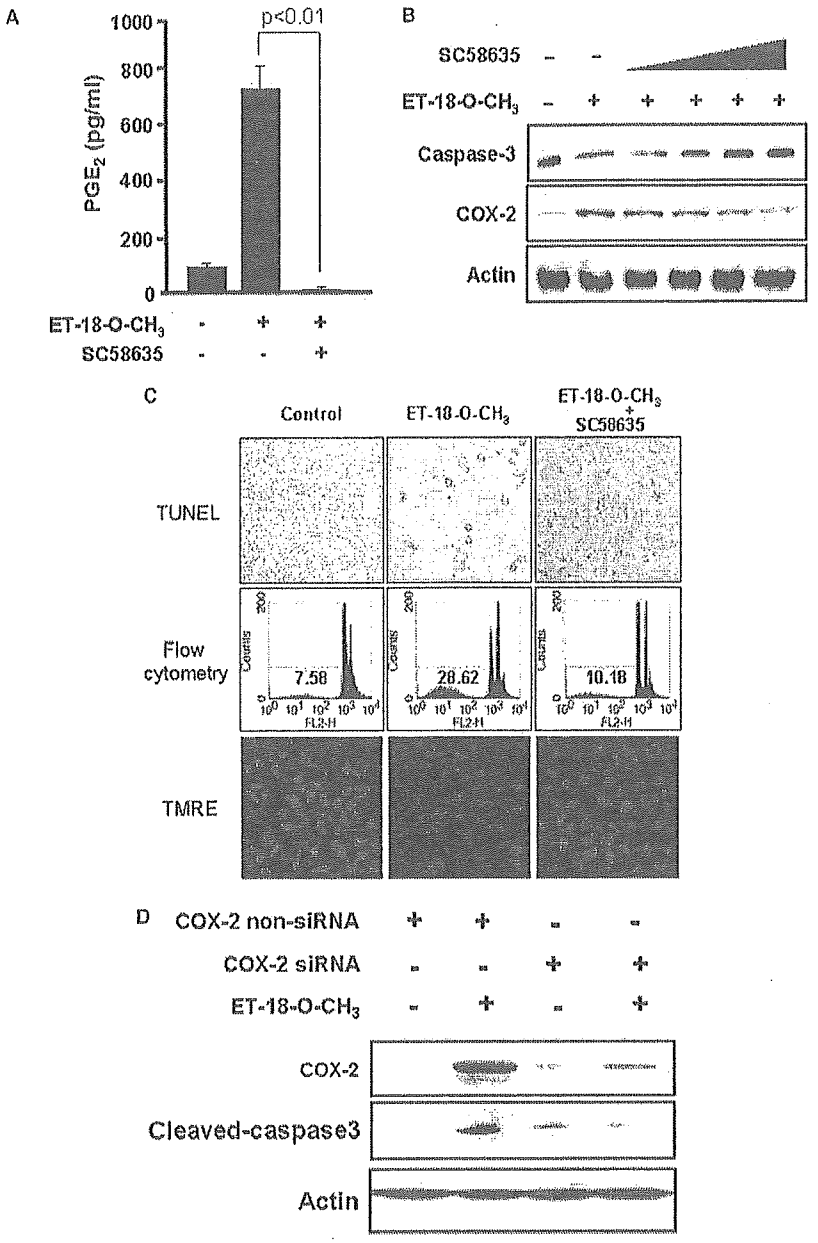

Fig. 3. Effects of the specific COX-2 inhibitor SC58635 on the ET-18-O-CH_3-induced apoptosis in MCF10A-*ras* cells. (A) Relative amount of PGE_2 released in the media following co-treatment of ET-18-O-CH_3 (2.5 μg/ml) for 3 days with SC58635 in the MCF10A-*ras* cells. (B) Effects of SC58635 on ET-18-O-CH_3-induced COX-2 expression as well as caspase-3 activation measured by Western blot analysis. MCF10A-*ras* cells were co-treated with ET-18-O-CH_3 (2.5 μg/ml) and 10, 25, 50 μM of SC58635 for 3 days. Protein extracts from the cells were immunoblotted with anti-COX-2, anti-caspase-3, and anti-actin antibodies. (C) SC58635 attenuation of ET-18-O-CH_3-induced apoptosis as determined by TUNEL, flow cytometry, and mitochondrial transmembrane permeability ($\Delta\psi_m$) changes. Cells were treated with ET-18-O-CH_3 (2.5 μg/ml) in the absence or presence of SC58635 (50 μM) for 1 day. (D) Effects of COX-2 siRNA on the ET-18-O-CH_3-induced COX-2 expression and cleaved PARP measured by Western blot analysis. MCF10A-*ras* cells were transfected with 20 nM non-specific and COX-2 specific siRNA before ET-18-O-CH_3 treatment.

to examine the products of COX-2. Among the COX-2-products, 15d-PGJ_2, an endogenous PPARγ ligand, has been known to possess pro-apoptotic potential in diverse cancer cells [40]. To examine whether 15d-PGJ_2 can mediate ET-18-O-CH_3-induced apoptosis, we measured the production of this cyclopentenone PG in the MCF10A-*ras* cells treated with ET-18-O-CH_3. 15d-PGJ_2 production was significantly elevated after treatment of ET-18-O-CH_3 (Fig. 5A). Again, SC58635 suppressed the production of 15d-PGJ_2 induced by ET-18-O-CH_3 (Fig. 5A). We also observed that exogenously added 15d-PGJ_2 inhibited the growth of MCF10A-*ras* cells (Fig. 5B) and induced apoptosis in MCF10A-*ras* cells as revealed by proteolytic cleavage of caspase-3 (Fig. 5C). As an endogenous ligand of PPARγ, 15d-PGJ_2 is likely to exert its biologic effects in part via PPARγ. Moreover, ET-18-O-CH_3 activated expression of PPARγ as well as COX-2 which preceded the activation of caspase-3 through proteolytic cleavage (Fig. 5D). We also observed that ET-18-O-CH_3 induced the

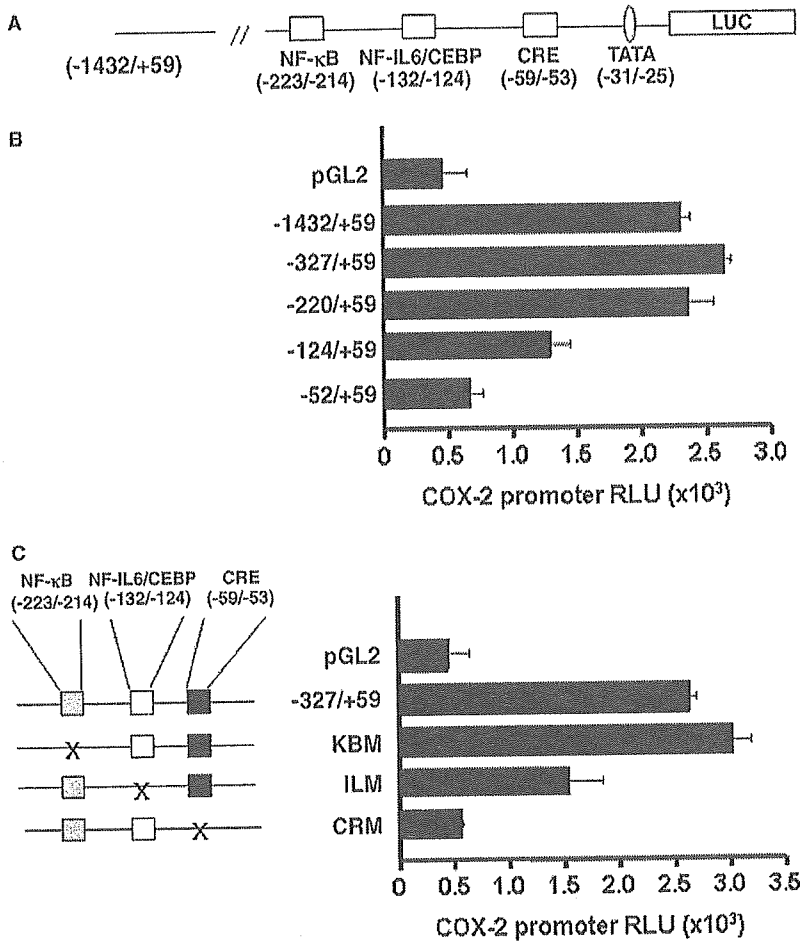

Fig. 4. ET-18-O-CH_3-induced activation of the COX-2 promoter. (A) A schematic representation of the human COX-2 promoter. (B) Determination of *cis*-acting elements of COX-2 promoter. MCF10A-*ras* cells were transfected with the 2.5 μg of a series of human COX-2 promoter deletion constructs (−1432/+59, −327/+59, −220/+59, −124/+59, −52/+59) ligated to luciferase. (C) Identification of the regions responsible for ET-18-O-CH_3-induced promoter activity of the human COX-2 gene. MCF10A-*ras* cells were transfected with 2.5 μg of a series of human COX-2 pormoter-luciferase constructs (−327/+59, KBM; ILM; CRM). KBM represents the −327/+59 COX-2 promoter construct in which the NF-κB site was mutated. ILM represents the −327/+59 COX-2 promoter construct in which the NF-IL6 site was mutated. CRM refers to the −327/+59 COX-2 promoter construct in which the CRE site was mutated. For the experiments related to B and C, MCF10A-*ras* cells were transiently co-transfected with pCOX-2 promoter and pCMV-β galactosidase (0.5 μg) for 24 h by using DOTAP Liposomal Transfection Reagent according to the manufacturer's instructions. Transfectant cells were treated with ET-18-O-CH_3 (2.5 μg/ml) for 4 h and the cells were lysed with reporter lysis buffer for measurement of luciferase activity. Luciferase activity represents data that have been normalized to β-galactosidase activity.

PPRE binding activity (Fig. 5E) and transcriptional activity (Fig. 5F) of PPARγ in MCF10A-*ras* cells. Therefore, ET-18-O-CH_3-induced COX-2 expression and subsequent production of 15d-PGJ_2 are likely to contribute to induction of apoptosis in MCF10A-*ras* cells.

4. Discussion

Multiple lines of evidence indicate that aberrant overexpression of COX-2 is implicated in inhibition of apoptosis and induced proliferation [2]. Tumor formation and growth are reduced in animals that are either genetically engineered to be COX-2 deficient or treated with a pharmacologic inhibitor of COX-2 [41–43]. The use of NSAIDs has been associated with a reduced risk of several malignancies through inhibition of COX-2 activity [44,45]. Moreover intake of the selective COX-2 inhibitor celecoxib reduced the burden of colorectal polyps in patients with familial adenomatous polyposis and has been shown to inhibit experimentally induced carcinogenesis [6,46,47]. Inhibition of COX-2 is hence recognized as one of the most feasible strategies for cancer chemoprevention and treatment.

Contrary to these findings, our present study clearly demonstrates that upregulation of COX-2 is causally linked to ET-18-O-CH_3-induced apoptosis in MCF10A-*ras* cells as a selective COX-2 inhibitor blocked the ET-18-O-CH_3-induced cell death. In this study, we found that mutation of the CRE binding site completely abolished the COX-2 promoter activity, suggesting that this site located in the COX-2 promoter plays a crucial role in regulating COX-2 transcription. Knock-down of COX-2 expression by siRNA also attenuated apoptosis induced by ET-18-O-CH_3. Other investigators have also reported that some of agents upregulate COX-2 expression while inducing apoptosis [7,48]. Thus, sphingosin 1-phosphate, a bioactive sphingolipid with growth-regulating properties,

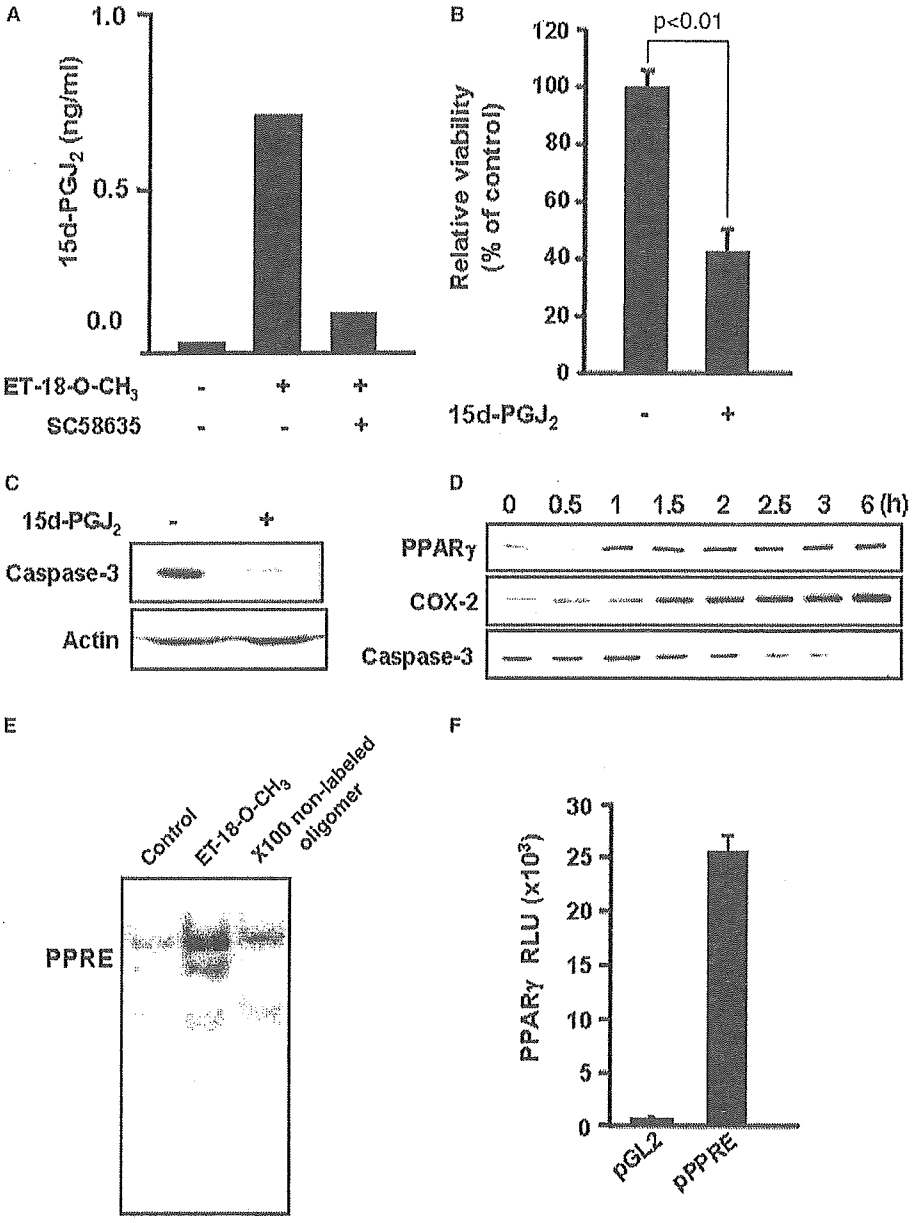

Fig. 5. Possible involvement of 15-PGJ_2 production in ET-18-O-CH_3-induced apoptosis. (A) Production of 15d-PGJ_2 in ET-18-O-CH_3 treated MCF10A-*ras* cells. The amounts of 15d-PGJ_2 released into media were measured after treatment of the cells with 2.5 μg/ml of ET-18-O-CH_3 for 1 days. (B) 15d-PGJ_2 induced anti-proliferative effect in MCF10A-*ras* cells. Cell viability was measured by the conventional MTT reduction assay after treatment with 15d-PGJ_2 (10 μM) for 1 day. Bars represent means ± S.E.M. of triplicate experiments. (C) 15d-PGJ_2 induced apoptosis in MCF10A-*ras* cells as evidenced by caspase-3 cleavage. (D) ET-18-O-CH_3 induced expression of PPARγ, COX-2, and caspase-3 cleavage as determined by immunoblot analysis. The concentration of ET-18-O-CH_3 was 2.5 μg/ml. (E) DNA-binding activity of PPARγ in ET-18-O-CH_3 treatment MCF10A-*ras* cells. Nuclear extracts were prepared from MCF10A-*ras* cells treated with ET-18-O-CH_3 for 30 min and incubated with the [γ-P^{32}] labeled oligonucleotide harboring PPRE, followed by electrophoretic mobility shifty assay. (F) Relative luciferase activity representing the transcriptional activity of PPARγ. MCF10A-*ras* cells were transiently co-transfected with pPPRE-Luc and pCMV-β galactosidase for 24 h using DOTAP Liposomal Transfection Reagent according to the manufacturer's instructions. Transfectant cells were treated with ET-18-O-CH_3 (2.5 μg/ml) for 6 h and the cells were lysed with reporter lysis buffer for the measurement of luciferase activity.

induced COX-2 expression and apoptosis, and blocking COX-2 by NS-398 blunted the anti-proliferative effect of sphingosin 1-phosphate in human hepatic myofibroblasts cells [7]. More recently, *R*(+)-methanandamide-induced cell death has been found to be associated with COX-2 upregulation in human neuroglioma cells [8]. Some of PGs are known to have proapoptotic activity. For instance, 15d-PGJ_2, a potent natural ligand for PPARγ, induces apoptosis in several types of cancer cells [49,50]. When MCF10A-*ras* cells were treated with exogenously added 15d-PGJ_2, this cyclopentenone PG induced apoptosis in MCF10A-*ras* cells. Moreover, ET-18-O-CH_3 treatment augmented production of 15d-PGJ_2. Biological effects of 15d-PGJ_2 could be elicited via several distinct mechanisms, either PPARγ-dependent or -independent. We found that ET-18-O-CH_3 induced expression of PPARγ and its subsequent binding to PPRE and transcriptional activity. It has

been reported that PPRE is located in the 5′ flanking region of the COX-2 promoter, and that induction of COX-2 expression by NSAIDs and PPARγ ligands is mediated via this element [51].

Besides COX-2-dependent induction of apoptosis we demonstrated in the present work, there might be other mechanisms which can also be attributable to ET-18-O-CH_3-induced apoptosis in MCF10A-*ras* cells. In this context, it is interesting to note that ET-18-O-CH_3-induced apoptosis is associated with production of reactive oxygen species in p53-defective hepatocytes [15] and HL-60 cells [28].

Blockade of ET-18-O-CH_3-induced apoptosis by SC58635 may have clinical implications. Recently, the chemotherapeutic agent paclitaxel-induced apoptosis in ovarian cancer cells, but combining treatment with COX-2 inhibitors resulted in a significant inhibition of paclitaxel-induced apoptosis, suggesting that combination of COX-2 inhibitors with chemotheraphy agents does not have an additive or synergistic tumoricidal effect [52]. If the same effect is true in vivo, the use of COX inhibitors prior to or concurrent with anticancer drug might carry a negative effect on therapeutic efficacy. Although COX-2 selective inhibitors are obviously have chemopreventive potential, it is necessary to examine carefully any adverse effects at the whole body level before considering their application for clinical.

In summary, COX-2 upregulation contributes to induction of apoptosis in MCF10A-*ras* cells treated with the anti-cancer drug ET-18-O-CH_3. These findings suggest that inhibition of COX-2 expression is not necessarily desirable for cancer prevention or therapy. It seems likely that the physiological functions of COX-2 depend on the types of inducers and cells, and targeted inhibition of COX-2 in the context of anticancer therapy may need more through validation.

Acknowledgment: This work was supported by Grant R02-2004-000-10197-0 from the Basic Research Program of the Korea Research Foundation (to Y.-J. Surh).

References

[1] DuBois, R.N., Awad, J., Morrow, J., Roberts II, L.J. and Bishop, P.R. (1994) Regulation of eicosanoid production and mitogenesis in rat intestinal epithelial cells by transforming growth factor-α and phorbol ester. J. Clin. Invest. 93, 493–498.

[2] Ishiko, O., Sumi, T., Yoshida, H., Matsumoto, Y., Honda, K., Deguchi, M., Yamada, R. and Ogita, S. (2001) Association between overexpression of cyclooxygenase-2 and suppression of apoptosis in advanced cancer of the uterine cervix after cyclic balloon-occluded arterial infusion. Oncol. Rep. 8, 1259–1263.

[3] Mohammed, S.I., Knapp, D.W., Bostwick, D.G., Foster, R.S., Khan, K.N., Masferrer, J.L., Woerner, B.M., Snyder, P.W. and Koki, A.T. (1999) Expression of cyclooxygenase-2 (COX-2) in human invasive transitional cell carcinoma (TCC) of the urinary bladder. Cancer Res. 59, 5647–5650.

[4] Cianchi, F., Cortesini, C., Bechi, P., Fantappie, O., Messerini, L., Vannacci, A., Sardi, I., Baroni, G., Boddi, V., Mazzanti, R. and Masini, E. (2001) Up-regulation of cyclooxygenase 2 gene expression correlates with tumor angiogenesis in human colorectal cancer. Gastroenterology 121, 1339–1347.

[5] Chun, K.S. and Surh, Y.J. (2004) Signal transduction pathways regulating cyclooxygenase-2 expression: potential molecular targets for chemoprevention. Biochem. Pharmacol. 68, 1089–1100.

[6] Chun, K.S., Kim, S.H., Song, Y.S. and Surh, Y.J. (2004) Celecoxib inhibits phorbol ester-induced expression of COX-2 and activation of AP-1 and p38 MAP kinase in mouse skin. Carcinogenesis 25, 713–722.

[7] Davaille, J., Gallois, C., Habib, A., Li, L., Mallat, A., Tao, J., Levade, T. and Lotersztajn, S. (2000) Antiproliferative properties of sphingosine 1-phosphate in human hepatic myofibroblasts. A cyclooxygenase-2 mediated pathway. J. Biol. Chem. 275, 34628–34633.

[8] Hinz, B., Ramer, R., Eichele, K., Weinzierl, U. and Brune, K. (2004) Up-regulation of cyclooxygenase-2 expression is involved in *R*(+)-methanandamide-induced apoptotic death of human neuroglioma cells. Mol. Pharmacol. 66, 1643–1651.

[9] Clay, C.E., Namen, A.M., Atsumi, G., Willingham, M.C., High, K.P., Kute, T.E., Trimboli, A.J., Fonteh, A.N., Dawson, P.A. and Chilton, F.H. (1999) Influence of J series prostaglandins on apoptosis and tumorigenesis of breast cancer cells. Carcinogenesis 20, 1905–1911.

[10] Li, L., Tao, J., Davaille, J., Feral, C., Mallat, A., Rieusset, J., Vidal, H. and Lotersztajn, S. (2001) 15-deoxy-Delta^{12,14}-prostaglandin J_2 induces apoptosis of human hepatic myofibroblasts. A pathway involving oxidative stress independently of peroxisome-proliferator-activated receptors. J. Biol. Chem. 276, 38152–38158.

[11] Shen, Z.N., Nishida, K., Doi, H., Oohashi, T., Hirohata, S., Ozaki, T., Yoshida, A., Ninomiya, Y. and Inoue, H. (2005) Suppression of chondrosarcoma cells by 15-deoxy-$\Delta^{12,14}$-prostaglandin J_2 is associated with altered expression of Bax/Bcl-xL and p21. Biochem. Biophys. Res. Commun. 328, 375–382.

[12] Berkovic, D. (1998) Cytotoxic etherphospholipid analogues. Gen. Pharmacol. 31, 511–517.

[13] Dimanche-Boitrel, M.T., Meurette, O., Rebillard, A. and Lacour, S. (2005) Role of early plasma membrane events in chemotherapy-induced cell death. Drug Resist. Updat. 8, 5–14.

[14] Slaton, J.W., Hampton, J.A. and Selman, S.H. (1994) Exposure to alkyllysophospholipids inhibits in vitro invasion of transitional cell carcinoma. J. Urol. 152, 1594–1598.

[15] Vrablic, A.S., Albright, C.D., Craciunescu, C.N., Salganik, R.I. and Zeisel, S.H. (2001) Altered mitochondrial function and overgeneration of reactive oxygen species precede the induction of apoptosis by 1-*O*-octadecyl-2-methyl-*rac*-glycero-3-phosphocholine in p53-defective hepatocytes. FASEB J. 15, 1739–1744.

[16] Na, H.K., Chang, C.C. and Trosko, J.E. (2003) Growth suppression of a tumorigenic rat liver cell line by the anticancer agent, ET-18-O-CH_3, is mediated by inhibition of cytokinesis. Cancer Chemother. Pharmacol. 51, 209–215.

[17] Candal, F.J., Bosse, D.C., Vogler, W.R. and Ades, E.W. (1994) Inhibition of induced angiogenesis in a human microvascular endothelial cell line by ET-18-OCH_3. Cancer Chemother. Pharmacol. 34, 175–178.

[18] Gajate, C., Fonteriz, R.I., Cabaner, C., Alvarez-Noves, G., Alvarez-Rodriguez, Y., Modolell, M. and Mollinedo, F. (2000) Intracellular triggering of Fas, independently of FasL, as a new mechanism of antitumor ether lipid-induced apoptosis. Int. J. Cancer 85, 674–682.

[19] Mollinedo, F., Martinez-Dalmau, R. and Modolell, M. (1993) Early and selective induction of apoptosis in human leukemic cells by the alkyl-lysophospholipid ET-18-OCH_3. Biochem. Biophys. Res. Commun. 192, 603–609.

[20] Shafer, S.H. and Williams, C.L. (2003) Non-small and small cell lung carcinoma cell lines exhibit cell type-specific sensitivity to edelfosine-induced cell death and different cell line-specific responses to edelfosine treatment. Int. J. Oncol. 23, 389–400.

[21] Civoli, F. and Daniel, L.W. (1998) Quaternary ammonium analogs of ether lipids inhibit the activation of protein kinase C and the growth of human leukemia cell lines. Cancer Chemother. Pharmacol. 42, 319–326.

[22] Powis, G., Seewald, M.J., Gratas, C., Melder, D., Riebow, J. and Modest, E.J. (1992) Selective inhibition of phosphatidylinositol phospholipase C by cytotoxic ether lipid analogues. Cancer Res. 52, 2835–2840.

[23] Ruiter, G.A., Verheij, M., Zerp, S.F. and van Blitterswijk, W.J. (2001) Alkyl-lysophospholipids as anticancer agents and enhancers of radiation-induced apoptosis. Int. J. Radiat. Oncol. Biol. Phys. 49, 415–419.

[24] Guo, H.B., Shen, Z.H., Huang, C.X., Ma, J., Huang, Y. and Chen, H.L. (2000) Modulation of the basal activity of phosphatidylinositol-3-kinase/protein kinase B signaling pathway in human hepatocarcinoma cells. Glycoconjugate J. 17, 315–322.

[25] Baburina, I. and Jackowski, S. (1998) Apoptosis triggered by 1-*O*-octadecyl-2-*O*-methyl-*rac*-glycero-3-phosphocholine is prevented by increased expression of CTP:phosphocholine cytidylyltransferase. J. Biol. Chem. 273, 2169–2173.
[26] Winkler, J.D., Eris, T., Sung, C.M., Chabot-Fletcher, M., Mayer, R.J., Surette, M.E. and Chilton, F.H. (1996) Inhibitors of coenzyme A-independent transacylase induce apoptosis in human HL-60 cells. J. Pharmacol. Exp. Ther. 279, 956–966.
[27] Surette, M.E., Winkler, J.D., Fonteh, A.N. and Chilton, F.H. (1996) Relationship between arachidonate–phospholipid remodeling and apoptosis. Biochemistry 35, 9187–9196.
[28] Gajate, C., Santos-Beneit, A.M., Macho, A., Lazaro, M., Hernandez-De Rojas, A., Modolell, M., Munoz, E. and Mollinedo, F. (2000) Involvement of mitochondria and caspase-3 in ET-18-OCH_3-induced apoptosis of human leukemic cells. Int. J. Cancer 86, 208–218.
[29] Mollinedo, F., Gajate, C., Martin-Santamaria, S. and Gago, F. (2004) ET-18-OCH3 (edelfosine): a selective antitumour lipid targeting apoptosis through intracellular activation of Fas/CD95 death receptor. Curr. Med. Chem. 11, 3163–3184.
[30] Gajate, C., Del Canto-Janez, E., Acuna, A.U., Amat-Guerri, F., Geijo, E., Santos-Beneit, A.M., Veldman, R.J. and Mollinedo, F. (2004) Intracellular triggering of Fas aggregation and recruitment of apoptotic molecules into Fas-enriched rafts in selective tumor cell apoptosis. J. Exp. Med. 200, 353–365.
[31] Inoue, H., Yokoyama, C., Hara, S., Tone, Y. and Tanabe, T. (1995) Transcriptional regulation of human prostaglandin-endoperoxide synthase-2 gene by lipopolysaccharide and phorbol ester in vascular endothelial cells. Involvement of both nuclear factor for interleukin-6 expression site and cAMP response element. J. Biol. Chem. 270, 24965–24971.
[32] Na, H.K. and Surh, Y.J. (2002) Induction of cyclooxygenase-2 in Ras-transformed human mammary epithelial cells undergoing apoptosis. Ann. N.Y. Acad. Sci. 973, 153–160.
[33] Chen, Z.H., Na, H.K., Hurh, Y.J. and Surh, Y.J. (2005) 4-Hydroxyestradiol induces oxidative stress and apoptosis in human mammary epithelial cells: possible protection by NF-κB and ERK/MAPK. Toxicol. Appl. Pharmacol. 208, 46–56.
[34] Gilhooly, E.M. and Rose, D.P. (1999) The association between a mutated ras gene and cyclooxygenase-2 expression in human breast cancer cell lines. Int. J. Oncol. 15, 267–270.
[35] Fujita, M., Fukui, H., Kusaka, T., Morita, K., Fujii, S., Ueda, Y., Chiba, T., Sakamoto, C., Kawamata, H. and Fujimori, T. (2000) Relationship between cyclooxygenase-2 expression and K-*ras* gene mutation in colorectal adenomas. J. Gastroenterol. Hepatol. 15, 1277–1281.
[36] Bissonnette, M., Khare, S., von Lintig, F.C., Wali, R.K., Nguyen, L., Zhang, Y., Hart, J., Skarosi, S., Varki, N., Boss, G.R. and Brasitus, T.A. (2000) Mutational and nonmutational activation of p21ras in rat colonic azoxymethane-induced tumors: effects on mitogen-activated protein kinase, cyclooxygenase-2, and cyclin D1. Cancer Res. 60, 4602–4609.
[37] Heasley, L.E., Thaler, S., Nicks, M., Price, B., Skorecki, K. and Nemenoff, R.A. (1997) Induction of cytosolic phospholipase A2 by oncogenic Ras in human non-small cell lung cancer. J. Biol. Chem. 272, 14501–14504.
[38] Howe, L.R., Subbaramaiah, K., Brown, A.M. and Dannenberg, A.J. (2001) Cyclooxygenase-2: a target for the prevention and treatment of breast cancer. Endocr. Relat. Cancer 8, 97–114.
[39] Inoue, H., Umesono, K., Nishimori, T., Hirata, Y. and Tanabe, T. (1999) Glucocorticoid-mediated suppression of the promoter activity of the cyclooxygenase-2 gene is modulated by expression of its receptor in vascular endothelial cells. Biochem. Biophys. Res. Commun. 254, 292–298.
[40] Na, H.K. and Surh, Y.J. (2003) Peroxisome proliferator-activated receptor γ (PPARγ) ligands as bifunctional regulators of cell proliferation. Biochem. Pharmacol. 66, 1381–1391.
[41] Oshima, M., Murai, N., Kargman, S., Arguello, M., Luk, P., Kwong, E., Taketo, M.M. and Evans, J.F. (2001) Chemoprevention of intestinal polyposis in the $Apc^{\Delta 716}$ mouse by rofecoxib, a specific cyclooxygenase-2 inhibitor. Cancer Res. 61, 1733–1740.
[42] Rao, C.V., Rivenson, A., Simi, B., Zang, E., Kelloff, G., Steele, V. and Reddy, B.S. (1995) Chemoprevention of colon carcinogenesis by sulindac, a nonsteroidal anti-inflammatory agent. Cancer Res. 55, 1464–1472.
[43] Oshima, H., Oshima, M., Inaba, K. and Taketo, M.M. (2004) Hyperplastic gastric tumors induced by activated macrophages in COX-2/mPGES-1 transgenic mice. EMBO J. 23, 1669–1678.
[44] Harris, R.E., Beebe-Donk, J. and Schuller, H.M. (2002) Chemoprevention of lung cancer by non-steroidal anti-inflammatory drugs among cigarette smokers. Oncol. Rep. 9, 693–695.
[45] Stockbrugger, R.W. (1999) Nonsteroidal anti-inflammatory drugs (NSAIDs) in the prevention of colorectal cancer. Eur. J. Cancer Prev. 8 (Suppl. 1), S21–S25.
[46] Phillips, R.K., Wallace, M.H., Lynch, P.M., Hawk, E., Gordon, G.B., Saunders, B.P., Wakabayashi, N., Shen, Y., Zimmerman, S., Godio, L., Rodrigues-Bigas, M., Su, L.K., Sherman, J., Kelloff, G., Levin, B. and Steinbach, G. (2002) A randomised, double blind, placebo controlled study of celecoxib, a selective cyclooxygenase 2 inhibitor, on duodenal polyposis in familial adenomatous polyposis. Gut 50, 857–860.
[47] Arico, S., Pattingre, S., Bauvy, C., Gane, P., Barbat, A., Codogno, P. and Ogier-Denis, E. (2002) Celecoxib induces apoptosis by inhibiting 3-phosphoinositide-dependent protein kinase-1 activity in the human colon cancer HT-29 cell line. J. Biol. Chem. 277, 27613–27621.
[48] Elder, D.J., Halton, D.E., Playle, L.C. and Paraskeva, C. (2002) The MEK/ERK pathway mediates COX-2-selective NSAID-induced apoptosis and induced COX-2 protein expression in colorectal carcinoma cells. Int. J. Cancer 99, 323–327.
[49] Siavash, H., Nikitakis, N.G. and Sauk, J.J. (2004) Targeting of epidermal growth factor receptor by cyclopentenone prostaglandin 15-deoxy-$\Delta^{12,14}$-prostaglandin J_2 in human oral squamous carcinoma cells. Cancer Lett. 211, 97–103.
[50] Eucker, J., Bangeroth, K., Zavrski, I., Krebbel, H., Zang, C., Heider, U., Jakob, C., Elstner, E., Possinger, K. and Sezer, O. (2004) Ligands of peroxisome proliferator-activated receptor γ induce apoptosis in multiple myeloma. Anticancer Drugs 15, 955–960.
[51] Pang, L., Nie, M., Corbett, L. and Knox, A.J. (2003) Cyclooxygenase-2 expression by nonsteroidal anti-inflammatory drugs in human airway smooth muscle cells: role of peroxisome proliferator-activated receptors. J. Immunol. 170, 1043–1051.
[52] Munkarah, A.R., Genhai, Z., Morris, R., Baker, V.V., Deppe, G., Diamond, M.P. and Saed, G.M. (2003) Inhibition of paclitaxel-induced apoptosis by the specific COX-2 inhibitor, NS398, in epithelial ovarian cancer cells. Gynecol. Oncol. 88, 429–433.

Quasi-monochromatic cerium flash angiography

Eiichi Sato*[a], Rudolf Germer[b], Etsuro Tanaka[c], Hidezo Mori[d], Toshiaki Kawai[e], Toshio Ichimaru[f], Shigehiro Sato[g], Hidenori Ojima[h], Kazuyoshi Takayama[h] and Hideaki Ido[i]

[a] Department of Physics, Iwate Medical University, 3-16-1 Honchodori, Morioka 020-0015, Japan
[b] ITP, FHTW FB1 and TU-Berlin, Blankenhainer Str. 9, D 12249 Berlin, Germany
[c] Department of Nutritional Science, Faculty of Applied Bio-science, Tokyo University of Agriculture, 1-1-1 Sakuragaoka, Setagaya-ku 156-8502, Japan
[d] Department of Cardiac Physiology, National Cardiovascular Center Research Institute, 5-7-1 Fujishirodai, Suita, Osaka 565-8565 Japan
[e] Electron Tube Division #2, Hamamatsu Photonics K. K., 314-5 Shimokanzo, Toyooka Village, Iwata-gun 438-0193, Japan
[f] Department of Radiological Technology, School of Health Sciences, Hirosaki University, 66-1 Honcho, Hirosaki 036-8564, Japan
[g] Department of Microbiology, School of Medicine, Iwate Medical University, 19-1 Uchimaru, Morioka 020-8505, Japan
[h] Shock Wave Research Center, Institute of Fluid Science, Tohoku University, 2-1-1 Katahira, Sendai 980-8577, Japan
[i] Department of Applied Physics and Informatics, Faculty of Engineering, Tohoku Gakuin University, 1-13-1 Chuo, Tagajo 985-8537, Japan

ABSTRACT

The cerium target plasma flash x-ray generator is useful in order to perform high-speed enhanced K-edge angiography using cone beams because K-series characteristic x rays from the cerium target are absorbed effectively by iodine-based contrast mediums. In the flash x-ray generator, a 150 nF condenser is charged up to 80 kV by a power supply, and flash x rays are produced by the discharging. The x-ray tube is a demountable diode, and the turbomolecular pump evacuates air from the tube with a pressure of approximately 1 mPa. Since the electric circuit of the high-voltage pulse generator employs a cable transmission line, the high-voltage pulse generator produces twice the potential of the condenser charging voltage. At a charging voltage of 80 kV, the estimated maximum tube voltage and current were approximately 160 kV and 40 kA, respectively. When the charging voltage was increased, the K-series characteristic x-ray intensities of cerium increased. The K lines were clean and intense, and hardly any bremsstrahlung rays were detected at all. The x-ray pulse widths were approximately 100 ns, and the time-integrated x-ray intensity had a value of approximately 10 μC/kg at 1.0 m from the x-ray source with a charging voltage of 80 kV. In the angiography, we employed a film-less computed radiography (CR) system and iodine-based microspheres.

Keywords: flash x-ray, cerium target, characteristic x rays, bremsstrahlung x-ray distribution, K-edge angiography

1. INTRODUCTION

The potential of monochromatic parallel x-ray beams using a synchrotron and a monochrometor poses a major challenge to competing image acquisition technology, for example, x-ray phase imaging[1,2] and enhanced K-edge angiography.[3,4] Recently, cone-beam phase imaging[5] for the edge enhancement technique has been employed using a mini-focus x-ray tube. Subsequently, K-edge angiography has also been performed using cone beams of cerium Kα rays[6] of 34.6 keV, since K-series characteristic x rays from the cerium target are absorbed effectively by iodine-based contrast media. Currently, most flash x-ray generators utilize cold-cathode x-ray tubes and produce extremely high-dose-rate pulse x rays with durations of less than 1 μs.[7] A number of flash x-ray generators have been developed in order to perform high-speed radiography, and the generators with maximum photon energies of less than 150 keV can be employed to

26th International Congress on High-Speed Photography and Photonics, edited by D. L. Paisley, S. Kleinfelder, D. R. Snyder, B. J. Thompson, Proc. of SPIE Vol. 5580 (SPIE, Bellingham, WA, 2005) · 0277-786X/05/$15 · doi: 10.1117/12.567575

perform soft radiography including biomedical applications.[8-12]
In a former experiment, we performed a preliminary experiment of high-speed K-edge angiography using a cerium plasma x-ray generator,[13] which produced both characteristic and bremsstrahlung x rays. As compared with a steady state x-ray generator with a constant tube voltage, the effective x-ray photon energies are lower, since both the tube voltage and current display damped oscillations; the tube current increases with decreasing tube voltage. Therefore, the condenser charging voltage should be increased as much as possible to increase the cerium characteristic x-ray intensity. In the present research, we improved a plasma x-ray generator[14-18] with a cerium-target tube, and used it to perform a preliminary study on angiography achieved with cerium K-series characteristic x rays.

2. PRINCIPLE OF K-EDGE ANGIOGRAPHY

Figure 1 shows the mass attenuation coefficients of iodine at the selected energies; the coefficient curve is discontinuous at the iodine K-edge. The average photon energies of the cerium Kα and Kβ lines are shown above the iodine K-edge. Cerium is a rare earth element and has a high reactivity; however, the average photon energy of Kα and Kβ lines are 34.6 and 39.2 keV, respectively, and iodine contrast media with a K-absorption edge of 33.2 keV absorb the lines easily. Therefore, blood vessels were observed with high contrasts.

3. GENERATOR

3.1 High-voltage circuit

Figure 2 shows a block diagram of a high-intensity plasma flash x-ray generator. The generator consists of the following essential components: a high-voltage power supply, a high-voltage condenser with a capacity of approximately 150 nF, an air gap switch, a turbomolecular pump, a thyratron pulse generator as a trigger device, and a flash x-ray tube. In this generator, a coaxial cable transmission line is employed in order to increase maximum tube voltage using high-voltage reflection. The high-voltage main condenser is charged up to 80 kV by the power supply, and electric charges in the condenser are discharged to the tube through the four cables after closing the gap switch with the trigger device.

3.2 X-ray tube

The x-ray tube is a demountable cold-cathode diode that is connected to the turbomolecular pump with a pressure of approximately 1 mPa (Fig. 3). This tube consists of the following major parts: a ring-shaped graphite cathode with an inside diameter of 4.5 mm, a stainless-steel vacuum chamber, a nylon insulator, a polyethylene terephthalate (Mylar) x-ray window 0.25 mm in thickness, and a rod-shaped cerium target 3.0 mm in diameter. The distance between the target and cathode electrodes can be regulated from the outside of the tube, and is set to 1.5 mm. As electron beams from the cathode electrode are roughly converged to the target by the electric field in the tube, evaporation leads to the formation of weakly ionized plasma, consisting of molybdenum ions and electrons, around the target. Because bremsstrahlung rays are not emitted in the opposite direction to that of electron acceleration (Fig. 4), cerium K-series characteristic x rays can be produced without using a filter.

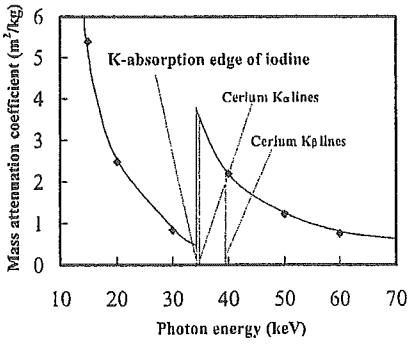

Figure 1: Relation between mass attenuation coefficient of iodine and average photon energies of cerium Kα and Kβ lines.

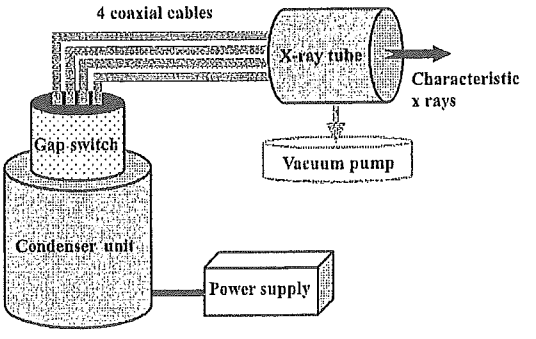

Figure 2: Block diagram of intense quasi-monochromatic flash x-ray generator.

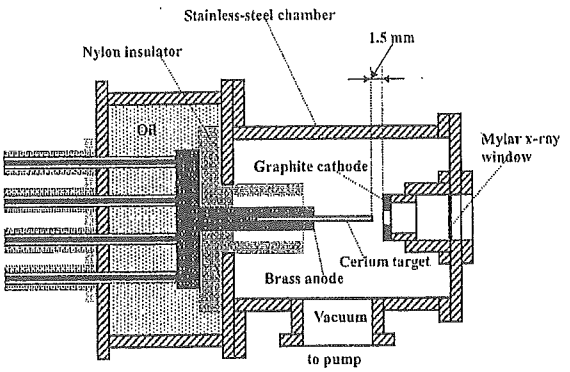

Figure 3: Schematic drawing of flash x-ray tube.

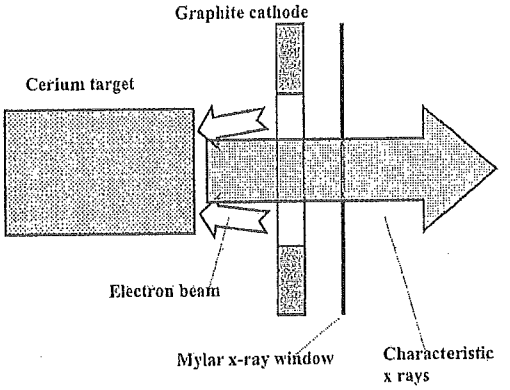

Figure 4: Irradiation of characteristic x rays.

4. CHARACTERISTICS

4.1 Tube voltage and current

In this generator, it was difficult to measure the tube voltage and current since the tube voltages were high, and there was no space to set a current transformer for measuring the tube current. Currently, the voltage and current roughly display damped oscillations. When the charging voltage was increased, both the maximum tube voltage and current increased. At a charging voltage of 80 kV, the estimated maximum values of the tube voltage and current were approximately 160 kV (2 times the charging voltage) and 40 kA, respectively.

4.2 X-ray output

X-ray output pulse was detected using a combination of a plastic scintillator and a photomultiplier (Fig. 5). The x-ray pulse height substantially increased with corresponding increases in the charging voltage. The x-ray pulse widths were approximately 100 ns, and the time-integrated x-ray intensity measured by a thermoluminescence dosimeter (Kyokko TLD Reader 1500 having MSO-S elements without energy compensation) had a value of approximately 10 μC/kg at 1.0 m from the x-ray source with a charging voltage of 80 kV.

4.3 X-ray source

In order to observe the Kα x-ray source, we employed a 100-μm-diameter pinhole camera and an x-ray film (Polaroid XR-7) (Fig. 6). When the charging voltage was increased, the plasma x-ray source grew, and both spot dimension and intensity increased. Because the x-ray intensity is the highest at the center of the spot, both the dimension and intensity decreased according to both increases in the thickness of a filter for absorbing x rays and decreases in the pinhole diameter.

4.4 X-ray spectra

X-ray spectra were measured by a transmission-type spectrometer with a lithium fluoride curved crystal 0.5 mm in thickness. The spectra were taken by a computed radiography (CR) system[19] with a wide dynamic range, and relative x-ray intensity was calculated from Dicom digital data. Figure 7 shows measured spectra from the cerium target. We observed clean K-series lines, while bremsstrahlung rays were hardly detected at all. The characteristic x-ray intensity substantially increased with increases in the charging voltage.

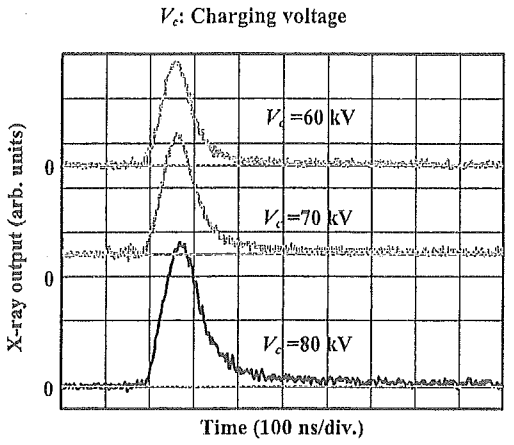

Figure 5: X-ray outputs at indicated conditions.

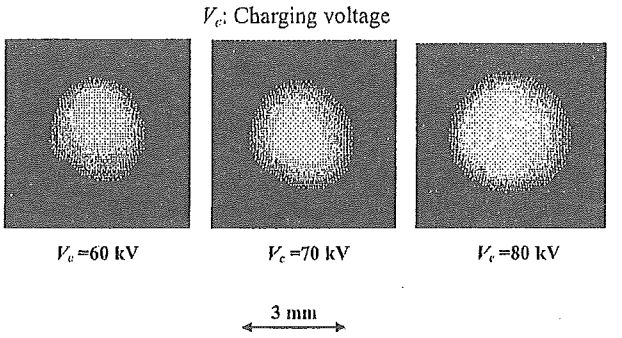

Figure 6: Images of characteristic x-ray source with changes in charging voltage.

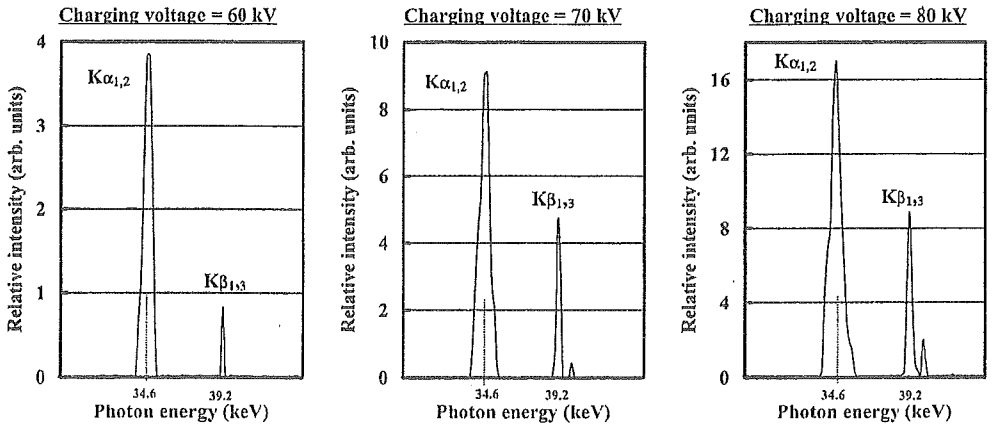

Figure 7: X-ray spectra from cerium target.

5. ANGIOGRAPHY

The plasma angiography was performed by the CR system (Konica Regius 150) without using a monochromatic filter, and the charging voltage and the distance between the x-ray source and the imaging plate were 70 kV and 1.2 m, respectively.

Figure 8 shows radiograms of tungsten wires coiled around a pipe made of polymethyl methacrylate. Although the image contrast increased with increases in the wire diameter, a 50 μm-diameter wire could be observed.

The image of water falling into a polypropylene beaker from a glass test tube is shown in Fig. 9. This image was taken with the slight addition of an iodine-based contrast medium. Because the x-ray duration was about 100 ns, the stop-motion image of water could be obtained.

Angiograms of rabbit hearts are shown in Fig. 10. These two images were obtained using iodine and cerium microspheres of 15 μm, respectively. In case where the cerium spheres were employed, the coronary arteries were barely visible. In angiography of a larger heart extracted from a dog using iodine spheres, fine blood vessels of approximately 100 μm were visible (Fig. 11).

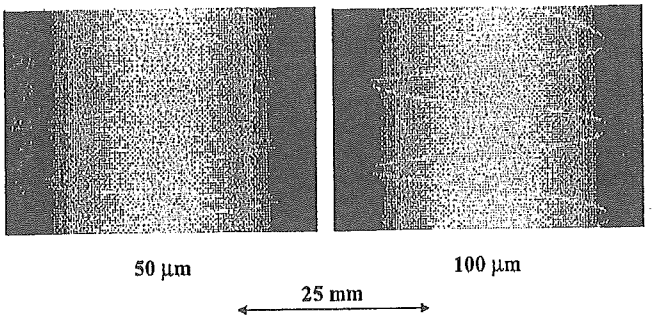

Figure 8: Radiograms of tungsten wires coiled around rod made of polymethyl methacrylate.

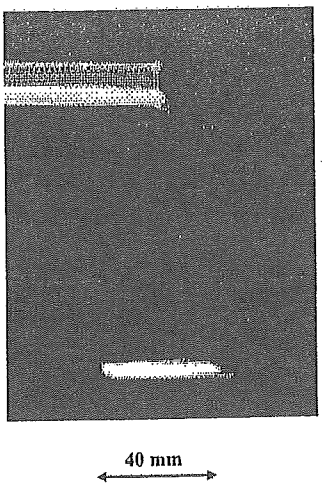

Figure 9: Radiogram of water falling into polypropylene beaker from glass test tube.

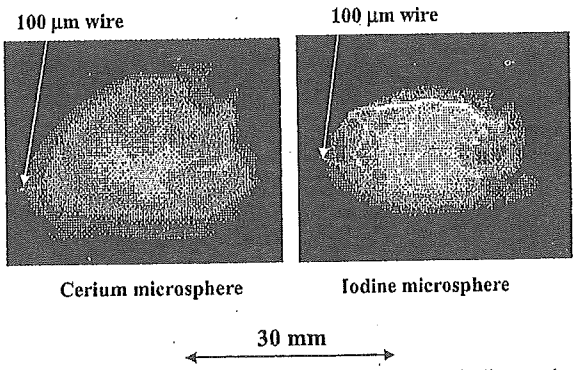

Figure 10: Angiograms of rabbit hearts using iodine and cerium microspheres.

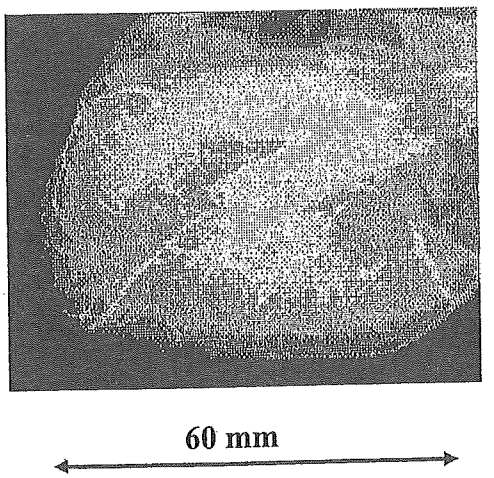

Fig. 11 Angiograms of extracted heart of dog.

6. DISCUSSION

Concerning the spectrum measurement, we obtained fairly clean cerium Kα and Kβ lines. Therefore, we are very interested in the measurement the characteristic rays from nickel, copper, molybdenum, silver, and tungsten targets; the target element should be selected corresponding to the radiographic objectives.

In this research, the generator produced instantaneous number of K photons was approximately 5×10^8 photons/cm^2 per pulse at 1.0 m from the source. Subsequently, the intensity can be increased by increasing the electrostatic energy in condenser, and monochromatic Kα lines are produced using a barium oxide filter with a barium K-edge of 37.4 keV.

Using this flash x-ray generator, as high output voltages can be produced using cables, high-photon-energy K-series characteristic x rays can be produced by increasing the atomic number of the target element. With recent advances in angiography using MRI, if the density of gadolinium-based contrast media increases, enhanced K-edge angiography

utilizing monochromatic x-ray generators, which produce Kα rays from ytterbium, tantalum, and tungsten targets, will be a useful technique to decrease the absorbed dose during angiography.

ACKNOWLEDGMENT

This work was supported by Grants-in-Aid for Scientific Research (13470154, 13877114, and 16591222) and Advanced Medical Scientific Research from MECSST, Health and Labor Sciences Research Grants(RAMT-nano-001, RHGTEFB-genome-005 and RHGTEFB-saisei-003), Grants from Keiryo Research Foundation, The Promotion and Mutual Aid Corporation for Private Schools of Japan, Japan Science and Technology Agency (JST), and New Energy and Industrial Technology Development Organization (NEDO, Industrial Technology Research Grant Program in '03).

REFERENCES

1. H. Mori, K. Hyodo, E. Tanaka, M. U. Mohammed, A. Yamakawa, Y. Shinozaki, H. Nakazawa, Y. Tanaka, T. Sekka, Y. Iwata, S. Honda, K. Umetani, H. Ueki, T. Yokoyama, K. Tanioka, M. Kubota, H. Hosaka, N. Ishizawa and M. Ando, "Small-vessel radiography in situ with monochromatic synchrotoron radiation," *Radiology*, **201**, 173-177, 1996.
2. K. Hyodo, M. Ando, Y. Oku, S. Yamamoto, T. Takeda, Y. Itai, S. Ohtsuka, Y. Sugishita and J. Tada, "Development of a two-dimensional imaging system for clinical applications of intravenous coronary angiography using intense synchrotron radiation produced by a multipole wiggler," *J. Synchrotron Rad.*, **5**, 1123-1126, 1998.
3. A. Momose, T. Takeda, Y. Itai and K. Hirano, "Phase-contrast x-ray computed tomography for observing biological soft tissues," *Nature Medicine*, **2**, 473-475, 1996.
4. M. Ando, A. Maksimenko, H. Sugiyama, W. Pattanasiriwisawa, K. Hyodo and C. Uyama, "A simple x-ray dark- and bright- field imaging using achromatic Laue optics, *Jpn. J. Appl. Phys.*, **41**, L1016-L1018, 2002.
5. A. Ishisaka, H. Ohara and C. Honda, "A new method of analyzing edge effect in phase contrast imaging with incoherent x-rays," *Opt. Rev.*, 7, 566-572, 2000.
6. E. Sato, E. Tanaka, H. Mori, T. Kawai, T. Ichimaru, S. Sato, K. Takayama and H. Ido, "Demonstration of enhanced K-edge angiography using a cerium target x-ray generator," *Med. Phys,* **31**, 3017-3021, 2004.
7. R. Germer, "X-ray flash techniques," *J. Phys. E: Sci. Instrum.*, **12**, 336-350, 1979.
8. E. Sato, S. Kimura, S. Kawasaki, H. Isobe, K. Takahashi, Y. Tamakawa and T. Yanagisawa, "Repetitive flash x-ray generator utilizing a simple diode with a new type of energy-selective function," *Rev. Sci. Instrum.*, **61**, 2343-2348, 1990.
9. A. Shikoda, E. Sato, M. Sagae, T. Oizumi, Y. Tamakawa and T. Yanagisawa, "Repetitive flash x-ray generator having a high-durability diode driven by a two-cable-type line pulser," *Rev. Sci. Instrum.*, **65**, 850-856, 1994.
10. E. Sato, K. Takahashi, M. Sagae, S. Kimura, T. Oizumi, Y. Hayasi, Y. Tamakawa and T. Yanagisawa, "Sub-kilohertz flash x-ray generator utilizing a glass-enclosed cold-cathode triode," *Med. & Biol. Eng. & Comput.*, **32**, 289-294, 1994.
11. K. Takahashi, E. Sato, M. Sagae, T. Oizumi, Y. Tamakawa and T. Yanagisawa, "Fundamental study on a long-duration flash x-ray generator with a surface-discharge triode," *Jpn. J. Appl. Phys.*, **33**, 4146-4151, 1994.
12. E. Sato, M. Sagae, E. Tanaka, Y. Hayasi, R. Germer, H. Mori, T. Kawai, T. Ichimaru, S. Sato, K. Takayama and H. Ido: Quasi-monochromatic flash x-ray generator utilizing a disk-cathode molybdenum tube, *Jpn. J. Appl. Phys.*, **43**, 7324-7328, 2004.
13. E. Sato, R. Germer, Y. Hayasi, K. Murakami, Y. Koorikawa, E. Tanaka, H. Mori, T. Kawai, T. Ichimaru, F. Obata, K. Takahashi, S. Sato, K. Takayama and Ido, H.: Weakly ionized cerium plasma radiography, *SPIE*, **5210**, 12-21, 2003.
14. E. Sato, Y. Hayasi, R. Germer, E. Tanaka, H. Mori, T. Kawai, H. Obara, T. Ichimaru, K. Takayama and H. Ido, "Intense characteristic x-ray irradiation from weakly ionized linear plasma and applications," *Jpn. J. Med. Imag. Inform. Sci.*, **20**, 148-155, 2003.
15. E. Sato, Y. Hayasi, R. Germer, E. Tanaka, H. Mori, T. Kawai, H. Obara, T. Ichimaru, K. Takayama and H. Ido, "Irradiation of intense characteristic x-rays from weakly ionized linear molybdenum plasma," *Jpn. J. Med. Phys.*, **23**, 123-131, 2003.
16. E. Sato, Y. Hayasi, R. Germer, E. Tanaka, H. Mori, T. Kawai, T. Ichimaru, K. Takayama and H. Ido, "Quasi-monochromatic flash x-ray generator utilizing weakly ionized linear copper plasma," *Rev. Sci. Instrum.*, 74, 5236-5240, 2003.
17. E. Sato, R. Germer, Y. Hayasi, Y. Koorikawa, K. Murakami, E. Tanaka, H. Mori, T. Kawai, T. Ichimaru, F. Obata, K. Takahashi, S. Sato, K. Takayama and H. Ido: Weakly ionized plasma flash x-ray generator and its distinctive characteristics. *SPIE*, **5196**, 383-392, 2003.